Faculteit Industriële Ingenieurswetenschappen

master in de industriële wetenschappen: chemie

Masterthesis

Optimization of hydrocarbon production through electrochemical reduction of CO2

Tim Henckens

Scriptie ingediend tot het behalen van de graad van master in de industriële wetenschappen: chemie

PROMOTOR :
Prof. dr. ir. Mumin Enis LEBLEBICI

BEGELEIDER :
ing. Tobias EL CHALID

Gezamenlijke opleiding UHasselt en KU Leuven

Universiteit Hasselt | Campus Diepenbeek | Faculteit Industriële Ingenieurswetenschappen | Agoralaan Gebouw H - Gebouw B | BE 3590 Diepenbeek

Universiteit Hasselt | Campus Diepenbeek | Agoralaan Gebouw D | BE 3590 Diepenbeek
Universiteit Hasselt | Campus Hasselt | Martelarenlaan 42 | BE 3500 Hasselt

2022
2023

Faculteit Industriële Ingenieurswetenschappen

master in de industriële wetenschappen: chemie

Masterthesis

Optimization of hydrocarbon production through electrochemical reduction of CO2

Tim Henckens

Scriptie ingediend tot het behalen van de graad van master in de industriële wetenschappen: chemie

PROMOTOR :

Prof. dr. ir. Mumin Enis LEBLEBICI

BEGELEIDER :

ing. Tobias EL CHALID

UHASSELT KU LEUVEN

Acknowledgements

I would like to express my gratitude to the individuals who played an important role in the completion of my master's thesis in chemical engineering. Their guidance, support, and expertise were instrumental in shaping and steering this project.

First and foremost, I would like to extend my appreciation to my daily mentor, Ing. Tobias El Chalid. Your commitment, invaluable insights, and constant encouragement throughout the research process were pivotal in driving this project forward.

I am also indebted to Prof. Dr. Mumin Enis Leblebici, my internal promotor, for his supervision and guidance throughout the entirety of this thesis. Your expertise and constructive feedback have been invaluable in shaping the direction and content of this research.

I would also like to extend my sincere thanks to Dr. Amer Hakki for his specific insights in electrochemistry. Your expertise in this specialized area of study provided crucial perspectives and contributed significantly to the development and understanding of the electrochemical aspects of my research. Your willingness to share your knowledge and offer guidance is genuinely appreciated.

Furthermore, I would like to express my gratitude to Marleen Segers for her assistance with the GC-MS analyses. Your expertise, meticulousness, and dedication to accuracy ensured the reliability and precision of the analytical data.

Lastly, I would like to express my deepest appreciation to my family and friends. Your support and encouragement have been the driving force behind my accomplishments.

Thank you all.

Table of contents

List of tables

Table of figures

List of symbols

PEC	Photoelectrochemical
ETR	Electron transfer rate
HER	Hydrogen evolution reaction
GDE	Gas diffusion electrode
MOF	Metal-organic framework
RE	Reference electrode
GC-MS	Gas chromatograph coupled to mass spectrometer

Abstract in English

The electrochemical reduction of CO_2 has the potential to play a vital role in addressing environmental challenges by reducing greenhouse gas emissions and generating valuable chemical feedstocks. This thesis aims to enhance the electrochemical reduction of CO_2 into CO and hydrocarbons through the optimization of reactor design, electrode configuration, external potential, and electrolyte selection.

Through the analysis of chrono amperometry measurements, an optimal reactor design has been achieved. This design features effective mixing accomplished through magnetic stirring in combination with continuous in-reactor CO_2 dissolution. Additionally, for optimal CO selectivity, the external potential was determined to be -1V (vs Ag/AgCl) in a KI electrolyte. Although chronoamperometry analysis has indicated the presence of a carbon reduction chain, the detection of hydrocarbons via GC-MS analysis has proven elusive. Consequently, it is recommended to implement liquid chromatograph analysis featuring a bonded-phase silica column with a low carbon loading (e.g., C_1 or C_2) in conjunction with a nonpolar mobile phase. The analysis setup should incorporate a Flame Ionization Detector (FID) for its high sensitivity to organic compounds.

Abstract in Dutch

De elektrochemische reductie van CO_2 heeft het potentieel om een cruciale rol te spelen bij het aanpakken van milieuproblemen door het verminderen van de uitstoot van broeikasgassen en het genereren van waardevolle chemische grondstoffen. Dit onderzoek heeft als doel de elektrochemische reductie van CO_2 tot CO en koolwaterstoffen te verbeteren door middel van optimalisatie van de reactorontwerp, elektrodeconfiguratie, externe potentiaal en elektrolytselectie.

Door middel van de analyse van chrono-amperometriemetingen is een optimaal reactorontwerp bereikt. Dit ontwerp omvat effectieve menging door middel van magnetisch roeren in combinatie met continue in-reactor CO_2-oplossing. Daarnaast is voor optimale CO-selectiviteit bepaald dat de externe potentiaal -1V (vs Ag/AgCl) moet zijn in een KI-elektrolyt. Hoewel de chrono-amperometrieanalyse de aanwezigheid van een koolstofreductieketen heeft aangegeven, is de detectie van koolwaterstoffen via GC-MS-analyse moeilijk gebleken. Daarom wordt aanbevolen om een vloeistofchromatografie-analyse uit te voeren met een gebonden-fase silica kolom met een lage koolstofbelasting (bijv. C_1 of C_2) in combinatie met een niet-polaire mobiele fase. De analyseopstelling dient tevens te worden voorzien van een vlamionisatiedetector (FID) vanwege de hoge gevoeligheid voor organische verbindingen.

1. Introduction

In this section, the context, problem definition, research objectives, and the corresponding plan of approach are outlined.

1.1 Context

Photoelectrochemical (PEC) applications can offer an environmentally friendly approach to help mitigate climate change problems. This through converting CO_2 into valuable chemicals and fuels, reducing reliance on fossil fuels and promoting a sustainable, carbon-neutral economy. In PEC reduction of CO_2, light energy is absorbed by a light-harvesting system, which is used to drive chemical reactions that produce energy-rich molecules. The most commonly used light-harvesting systems are composed of semiconductor materials, such as Si, TiO_2, and ZnO_2 [1,2,3,6,7]. Figure 1 shows a simplified scheme of a typical PEC reduction of CO_2 in an H-Cell.

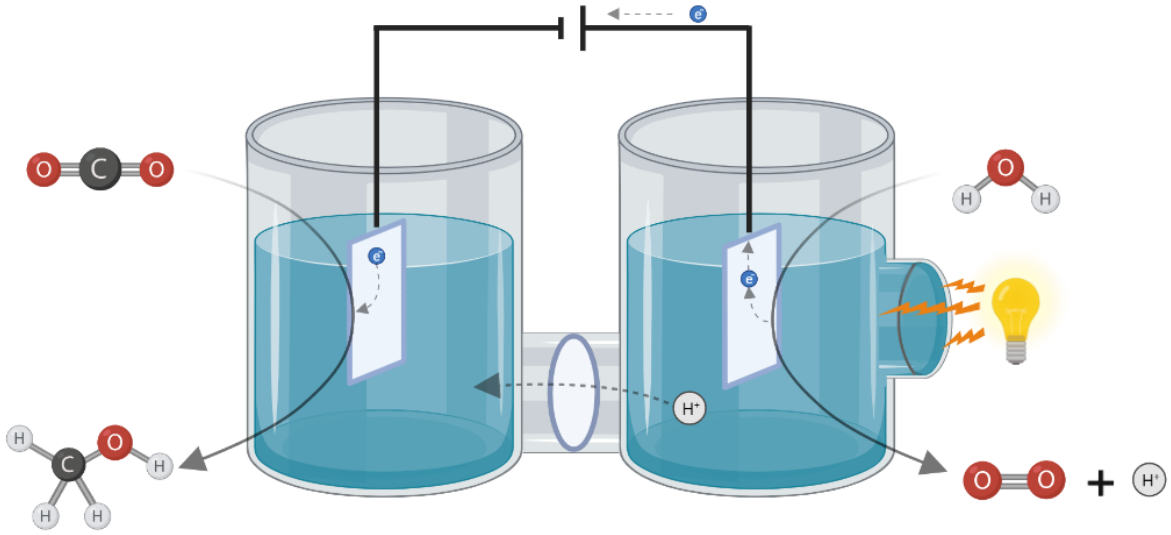

Figure 1 Simplified scheme of a photoelectrochemical reduction of carbon dioxide in a H-Cell.

The general working principle of a PEC involves the absorption of above band gap energy irradiated photons by the semiconductor. The absorbed photons will excite an electron of the semiconductor material creating an electron-hole pair. After the formation of these electron hole pairs, an electron can either recombine with a positive hole or be transferred to an active (surface) reaction site where it reacts with CO_2 [4,5]. The remaining positive holes will act as a driving force for water oxidation reactions at the anodic catalyst reaction sites. Here, a photocatalyst can also be used to produce electron hole pairs. However, the positive holes now present the driving force for the oxidation of water. The electrons are then conducted to cathode and can effectively neutralize the cathodic positive holes. It is important to mention that often an additional external potential supply is implemented to increase the kinetics of the redox reactions. Due to differences in (photo-)catalyst, electrolyte, pH and CO_2 saturation levels, a wide range of reaction products has been reported. However, exact mechanisms are still subject to debate. Figure 2 provides a simplified reaction mechanism scheme for different hydrocarbons:

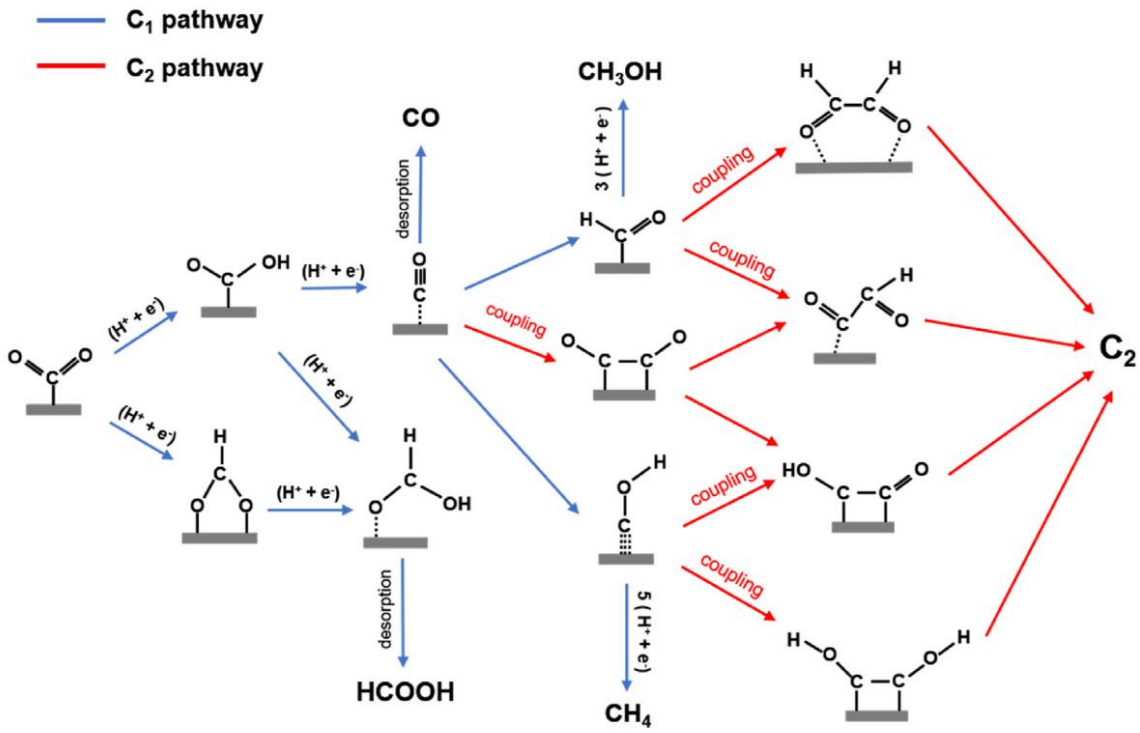

Figure 2 Simplified CO2 reduction mechanisms and reaction products [8].

The ability to produce these molecules in a renewable and sustainable manner has significant implications for the development of sustainable energy-dense molecules [6].

Although the potential benefits of photoelectrochemical reduction of CO_2, there are still several challenges and limitations that need to be addressed. These include competition of the hydrogen evolution reaction (HER), low reaction rates, poor selectivity, and limited scalability of the process. In addition, the development of efficient and stable catalysts is a major challenge for the photoelectrochemical reduction of CO_2 [9]. Moreover, optimizing the reactor design to maximize light absorption and minimize mass transport limitations is also critical for improving the overall efficiency of the process.

In conclusion, the photoelectrochemical reduction of CO_2 has the potential to revolutionize the energy sector and mitigate climate change. However, current limitations and challenges need to be overcome through extensive research on efficient and stable catalysts, optimized reactor designs, and improved transfer phenomena.

1.2 Problem definition

Although research has been conducted on this topic, several challenges hinder the widespread implementation of PEC systems. This is caused by multiple shortcomings.

The first issue is presented by the formation of a concentration gradient along the (photo-)catalysts, this can effectively create film diffusion limitations. Extensive mixing of the electrolytes is necessary to address this issue. Catalyst design is the second challenge, as the efficiency of the water oxidation and carbon dioxide reduction reactions largely depends on the catalysts used. The most efficient catalysts currently available, such as Au or Pt, are expensive and require rare metals, which limits their scalability [2]. Electrode selectivity in CO_2 reduction reactions is crucial for high efficiency and product selectivity, impacting both energy efficiency and yield. One common by-product is H_2, which can significantly decrease the efficiency of hydrocarbon production. Additionally, there are challenges regarding (photo-)catalyst selection. The development of efficient and stable catalysts that can operate under practical conditions is crucial for practical application. Many PEC catalysts are prone to degradation under prolonged illumination or exposure to reactive environments, which limits their practical application. Furthermore, optimal catalyst selectivity is crucial for large scale industrial applications. Thirdly, electrolyte selection can significantly affect both CO_2 solubility and hydrocarbon selectivity. Electrolytes consist of NaCl, Na_2SO_4, $NaHCO_3$/Na_2CO_3 or KI mixtures [10-12]. Lastly, energy efficiency is a challenge as the amount of energy needed to drive the water splitting and carbon dioxide reduction reactions is relatively high, and this energy must be produced by renewable sources to make the process truly sustainable.

By addressing these challenges, it becomes possible to provide insights for the development of efficient and scalable PEC systems for sustainable production of short-chain carbohydrates.

1.3 Research objectives

The objective of this research project is to optimize (photo-)electrochemical systems for the efficient production of carbohydrates from CO_2 at a pilot scale. To achieve this main objective, several strategies will be employed, which can be categorized into three main groups: material selection, system design, and reaction conditions. In terms of material selection, the objective is to compare the efficiency, selectivity, and stability of different cathodic photoelectrocatalysts materials such as Au, Cu and Pt.

Regarding system design, the first objective is to test different electrolytes in order to enhance the efficiency and selectivity of the CO_2 reduction process by. The second objective is to assess the effects of external CO_2 dissolving and recycling of reactor contents to maximize CO_2 saturation degree and minimize diffusion limitations respectively.

Concerning reaction conditions, the first objective is to adjust the reaction conditions, such as applied external voltage, to optimize the selectivity of the CO_2 reduction process. The second objective is to investigate how tuning the pH can shift the selectivity towards CO or hydrocarbons.

1.4 Plan of approach

The research objectives are chronologically investigated to optimize the (photo-)electrochemical reduction of CO_2. It is divided into several subsections, each focusing on specific aspects of the research.

The primary objective of the study is to investigate various aspects related to the improvement of reduction current density and current stability in the reactor configuration. This entails conducting in-depth examinations to optimize film diffusion, CO_2 dissolution, and electrocatalyst configuration. In a subsequent phase, the investigation will explore how the external potential effects the current density and selectivity of the process. Through experimentation, the relationship between different external potentials and the resulting changes in current density and selectivity will be examined. Furthermore, the effects of different electrolytes on the electrochemical reactions will be analyzed. The performance of each electrolyte and assessing their impact on reaction kinetics and product selectivity will be assessed. In addition, the influence of TiO_2 electrocatalyst thickness on the (photo-)electrochemical reduction of CO_2 will be examined. The thickness of the TiO_2 layer will be varied and its impact on the reaction kinetics analyzed, aiming to identify the optimal TiO_2 layer thickness to reach a maximum current density.

Throughout the optimization research, the study will diligently provide experimental data, figures, and analysis to support the findings. The organization of the subsections will ensure a comprehensive understanding of the ongoing optimization studies for the electrochemical reduction of CO_2.

2. Theoretical background information

2.1 CO_2 reduction mechanisms

The formation of reaction products during CO_2 reduction can be influenced by various factors, such as (photo-)catalyst type, pH, and electrolyte. Although some reaction mechanisms have been studied experimentally, most are based on density functional theory calculations due to their complexity [10]. Thus, the mechanisms that are discussed are not necessarily complete and further research is needed to determine the exact mechanisms.

2.1.1 CO_2 activation

The first electron transfer reaction (ETR) in the electrochemical reduction of CO_2 is the activation step. An ETR occurs when electrons are transferred between two atoms or molecules [11,12]. In this case, the electrons are transferred between the catalyst surface and a CO_2 molecule. Firstly, the CO_2 molecule is adsorbed onto the surface of the electrode. It is then activated through the transfer of electrons from the electrode. This results in the formation of intermediates such as CO_2^-, CO_3^{2-}, and HCO_3^- [13]. These intermediates can then undergo further reduction to form various products via different pathways. However, the activation energy is relatively high, this implies that catalyst choice is crucial for achieving hydrocarbon selectivity.

2.1.2 CO formation

The formation of CO is often reported during the electrochemical reduction of CO_2 [14,15]. CO formation is an important reaction because it represents a potential intermediate product for the synthesis of further reduced carbon reaction products. The reduction of CO_2 to CO can occur through several possible mechanisms and depend on the catalysts used and applied reaction conditions. The most common and straightforward mechanisms for the formation of CO involves the transfer of two electrons to CO_2 to form CO and H_2O. This reaction can occur through several possible pathways, which can involve intermediates such as formate [16]. Figure 3 provides a simplified overview of the formation mechanisms of CO.

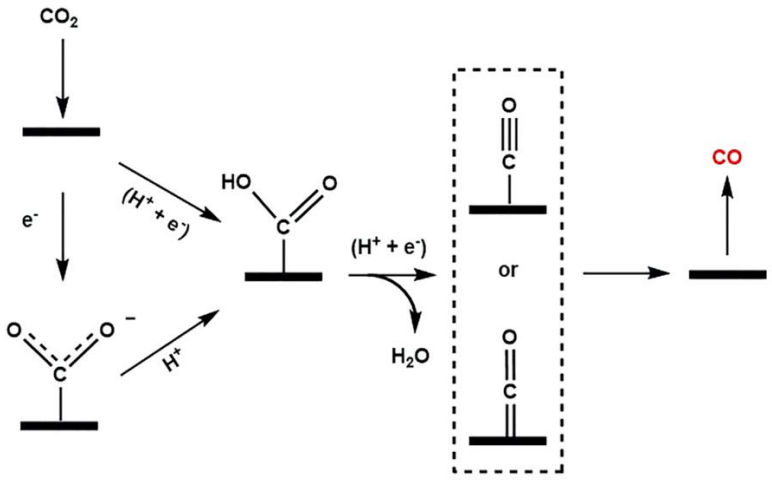

Figure 3 Formation pathways of carbon monoxide [17]

The selectivity towards CO can be tuned by controlling the reaction conditions. The most important parameters are the temperature and pressure of the system, (photo-)catalyst type, as well as the intensity and wavelength of the light [16].

2.1.3 Formate formation

Formate ($HCOO^-$) is one of the major products that can be formed during the electrochemical reduction of CO_2. The formation of formate is an important reaction in the overall process of CO_2 reduction, as it represents a potential intermediate product for the synthesis of various chemicals and fuels. The reduction of CO_2 to formate can occur through several possible mechanisms, which depend on the catalysts and reaction conditions used. One of the most common mechanisms for the formation of formate involves the transfer of two electrons and two protons to CO_2 to form formic acid, which can then be further deprotonated to form $HCOO^-$. Figure 4 gives an overview of different reaction mechanisms leading to the formation of $HCOO^-$.

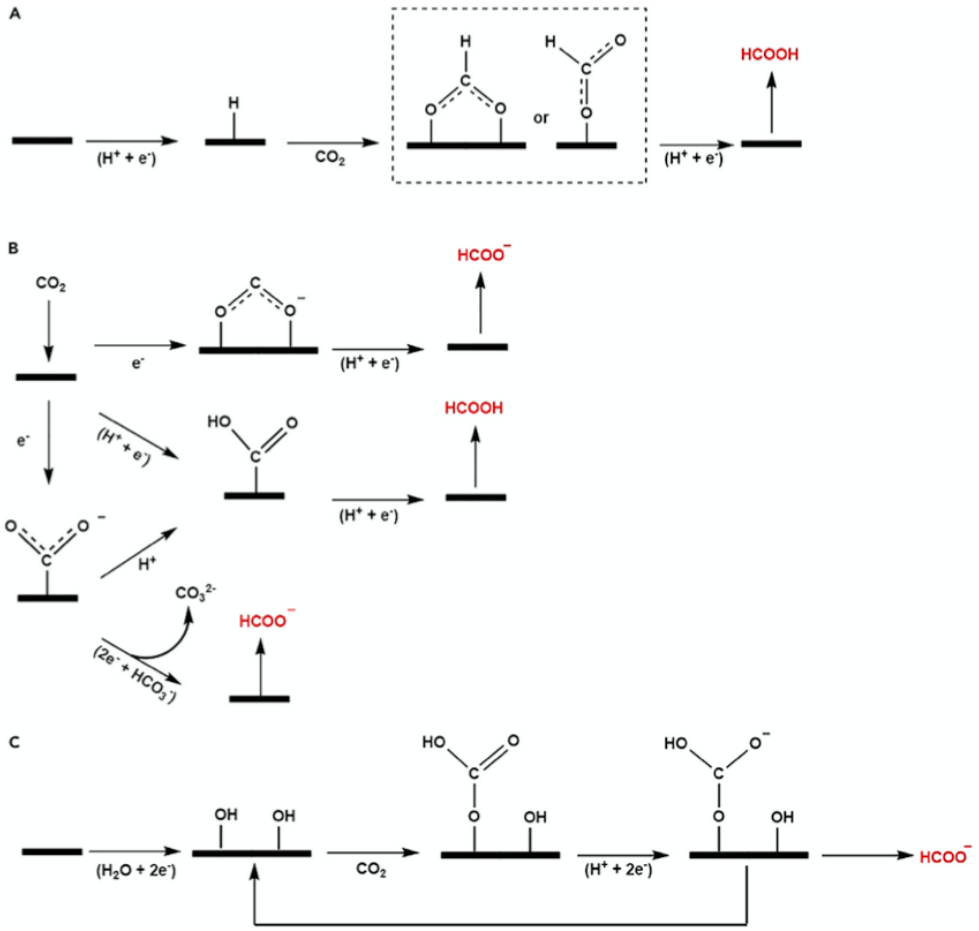

Figure 4 Formation pathways of formate and formic acid [17], (A) Monodentate or bidentate intermediate route [18], (B) CO_2^- radical intermediate route [16], (C) Surface-bound carbonate intermediate route [19]

Typically, this reaction is facilitated using catalysts consisting of titanium, cadmium, indium, as well as other metals. The selectivity towards formate can be adjusted by changing pH, electrolyte, and the catalyst. For example, a higher pH value will promote formate formation [20].

2.1.4 Methane, methanol, and formaldehyde formation

Methane, methanol, and formaldehyde are other products that can be formed during electrochemical reduction of CO_2. Several reduction mechanisms have been proposed. These often depend on the (photo-)catalyst, pH, and other reaction conditions. Methane formation from CO_2 generally involves the transfer of 8 electrons and 8 protons. Methanol is another intermediate product which involves the transfer of 6 electrons and 6 protons. Formaldehyde on the other hand, requires two electrons and two protons to form formic acid, which is subsequently dehydrated to form formaldehyde. Figure 5 gives an overview of methane, methanol, and formaldehyde formation mechanisms.

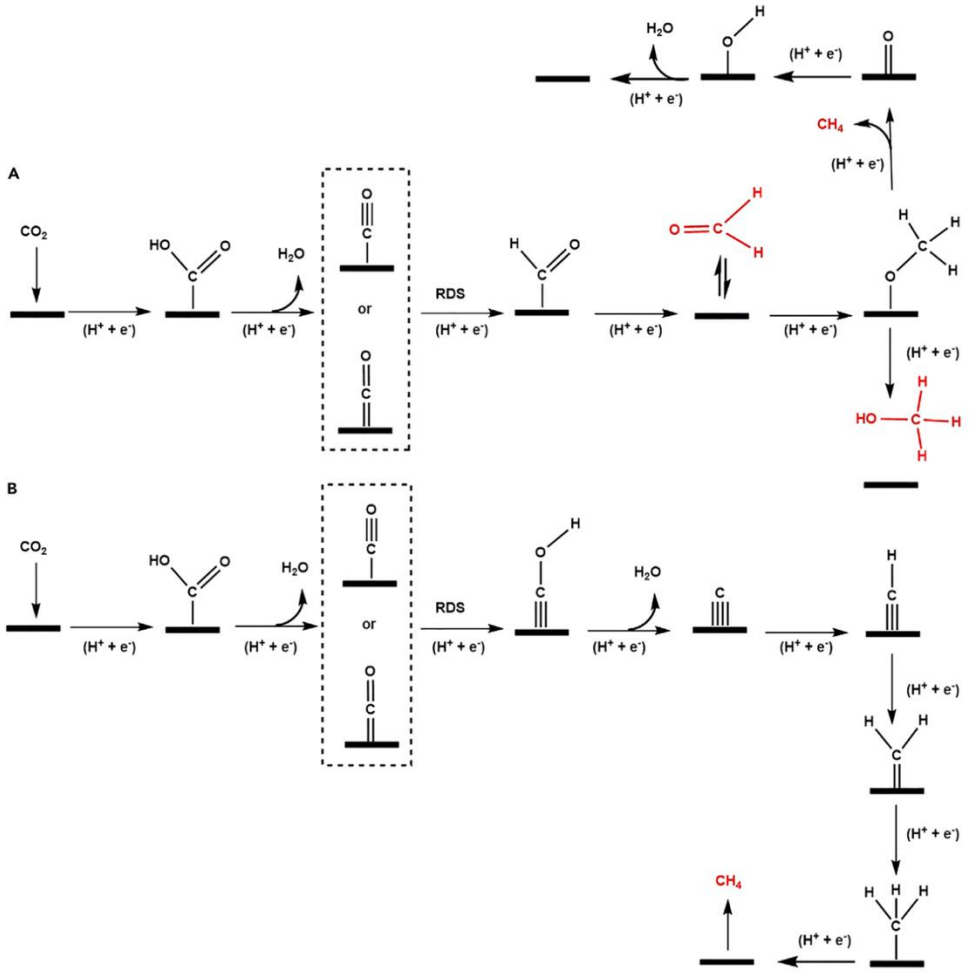

Figure 5 Formation mechanisms of methane, methanol, and formaldehyde [17], (A) Thermodynamic analysis [21], (B) Combined thermodynamic and kinetic analysis [22].

The production of these hydrocarbons has been observed mainly on metallic and oxidized copper electrodes [21-25]. Each reaction step involves the consumption of protons and electrons. This indicates that selectivity is highly dependent on pH, external potential, and electrocatalyst geometry.

2.1.5 Ethane, ethanol, and acetaldehyde formation

The formation of C-C bonds during electrochemical reduction of CO_2 has been reported in some cases when copper-based electrodes are used. The formation of C_2-products such as ethene, ethanol or acetaldehyde can be attributed to different geometric structures of the active catalytic sites of copper electrocatalysts. The exact formation mechanisms of C-C bonds are still subject to debate. However, one proposal suggests that adjacent regions of metallic copper and cuprous oxide (Cu_2O) can be responsible for this behaviour [14]. Figure 6 gives an overview of the general C-C bond mechanism that is proposed.

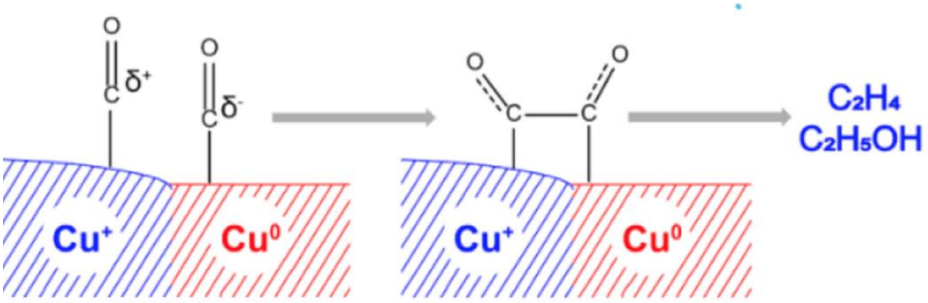

Figure 6 General C-C bond formation mechanism proposed by Shang et al. [14].

The reaction mechanisms for ethene are complex and depend on different factors such as type of copper electrocatalyst, pH and other reaction conditions. Also, the involvement of intermediate species, such as formic acid and CO is suspected. Furthermore, a final dimerization reaction is necessary. However, the exact mechanisms are still unknown and further research is necessary.
The formation of ethanol on the other hand, consists of complex mechanisms and involves several different pathways. It is suspected that it first involves the formation of formic acid, methanol, and acetaldehyde.

Lastly, acetaldehyde is another product that can be formed during the electrochemical reduction of CO_2 on copper-based electrocatalysts. The formation of acetaldehyde is believed to occur through the reduction of CO_2 to formate, which is then further reduced to acetaldehyde. This reaction pathway is thought to involve the adsorption of formate and the subsequent reduction of the adsorbed species. The exact mechanism of this reaction is still under investigation, but it has been suggested that the formation of acetaldehyde is promoted by the presence of copper oxide or copper hydride species on the catalyst surface. Figure 7 gives an overview of different reaction mechanisms leading to the formation of ethane, ethanol, and acetaldehyde.

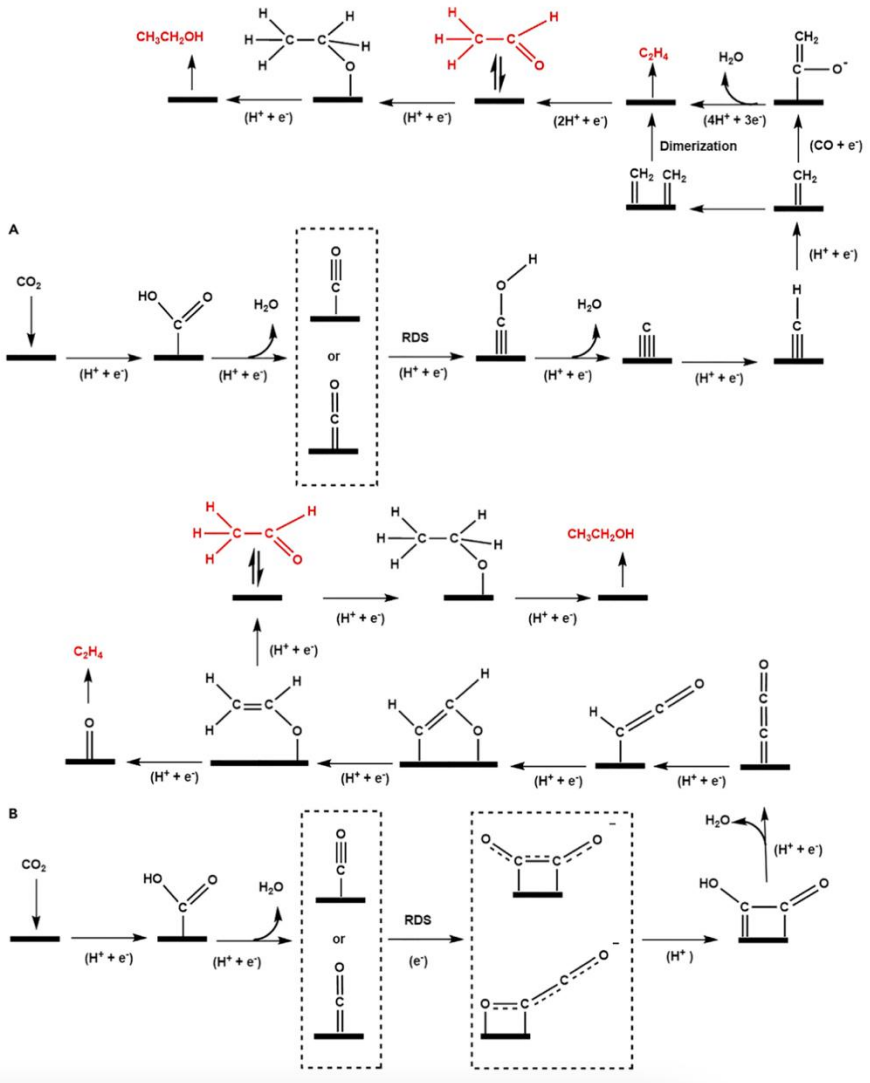

*Figure 7 Formation mechanisms of ethane, ethanol, and acetaldehyde [17], (A) Coupling of two ˙CH2 species or CO insertion [26], (B) *CO dimerization [27].*

The formation mechanisms of acetaldehyde, ethylene, and ethanol during the electrochemical reduction of CO_2 are complex and depend on various factors. The selectivity and efficiency of these products can be enhanced by optimizing the reaction conditions and using suitable catalysts, which can have important applications in the synthesis of various chemicals and fuels.

2.2 Hydrogen gas formation

H_2 formation is a competitive reaction that can occur during the electrochemical reduction of CO_2. H_2 can be synthesized as a by-product and is formed through the reduction of protons [9].

$$2H^+ + 2e^- \rightarrow H_2$$

This reaction equation shows that it only requires two protons and electron, in contrast to most of the hydrocarbon reaction products. Due to the relative simplicity of the hydrogen formation reaction and significantly fewer intermediate products compared to hydrocarbon formation, the reaction often presents the main competing reaction for CO_2 reduction products.

Although the formation of hydrogen gas is reported in a wide range of process conditions, the selectivity towards hydrogen gas production is highly dependent on the pH of the electrolyte and the applied potential [28]. Typically, a lower pH-value combined with lower overpotentials favour hydrogen formation, while higher, alkaline pH-values combined with higher overpotentials favour the reduction of carbonaceous products [28]. Additionally, the selectivity towards HER can be influenced by (photo-)catalyst material. For example, platinum or palladium electrodes exhibit a high selectivity, while copper exhibits a low selectivity towards H_2 formation [9].

Furthermore, the selectivity towards H_2 formation can also be influenced by the presence of co-catalysts or additives in the electrolyte. For example, the addition of certain organic acids or alcohols can increase selectivity by stabilizing protons and promoting their reduction. Similarly, the use of co-catalysts, such as cobalt or nickel, can also increase selectivity by facilitating the reduction of protons [29].

2.3 Reactor design

Currently, different reactor designs are successfully implemented for lab scale research. Each design has specific advantages and disadvantages. Reactor design significantly influences the efficiency of the process. Optimally, the reactor design must optimize photon transport, electron transport and mass transport. Furthermore, to ensure stability, reactor materials need to be carefully considered.

2.3.1 H-type reactor

H-type cells are the least complex reactors, their name originates from the visual similarity with the letter "H". H-type reactors consist of two compartments, namely an anodic and cathodic one. The contents of these compartments are often separated by a conductive membrane to ensure ionic conductivity, while the catholyte and anolyte remain separated. Figure 8 shows a schematic overview of a typical H-type reactor design.

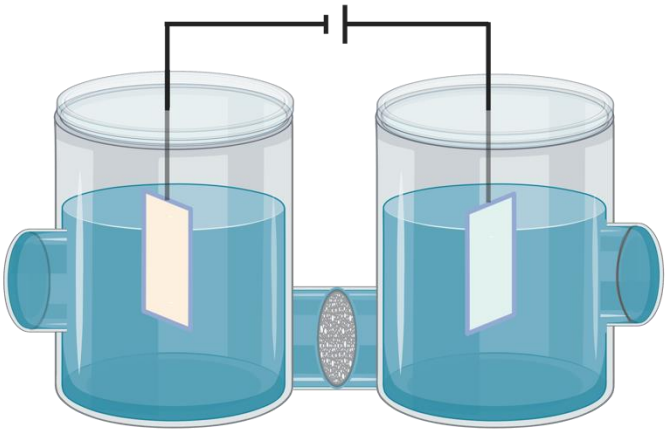

Figure 8 Schematic representation of a H-type cell reactor

The main advantage of this reactor design type is its simplicity. However, this is contrasted by several shortcomings. The main disadvantage is that it is not able to run continuously, it is thus often used for (semi) batch processes. Furthermore, H-type reactors often require relatively high reactor volumes, while dissolved CO_2 concentrations are relatively low. This can lead to increased distance between the electrodes and mass transport limitations [30].

2.3.2 Gas diffusion electrode reactor

Gas diffusion electrodes (GDEs) are often implemented in CO_2 reduction experiments to address the poor CO_2 solubility in most aqueous electrolytes. A GDE consists of several layers, where the catalyst is deposited on multiple gas permeable substrates. When this type of electrode is used in CO_2 reduction experiments, it serves as a cathode where CO_2 gas can diffuse through the porous gas permeable layers to the actual cathodic catalyst [32]. Figure 9 shows a schematic representation of a typical GDE when it is applied during the electrochemical reduction of CO_2.

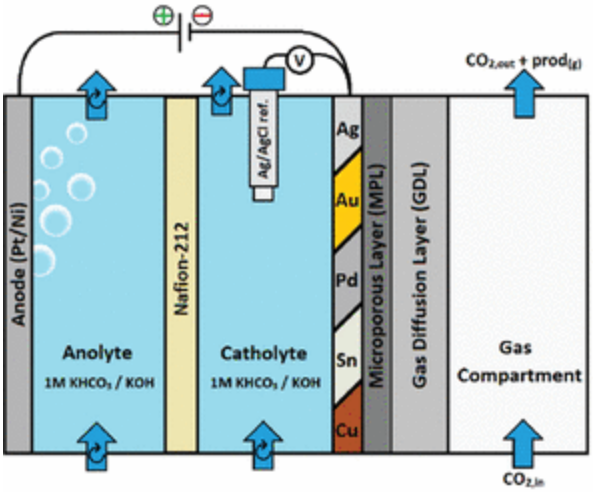

Figure 9 Schematic representation of a gas diffusion electrode reactor for CO2 reduction [33]

The application of GDEs exhibits multiple advantages over classical methods such as CO_2 dissolution in aqueous electrolytes. The first and foremost advantage is the relatively efficient mass transfer of CO_2 to the cathode, resulting in higher reduction rates. Secondly, GDEs exhibit relatively high catalyst surface area which can also increase reduction rates. Lastly, they are relatively low cost due to their simple design and show significant potential for large-scale, industrial applications [34].

2.3.3 Flow reactor

Flow reactors are becoming increasingly popular for CO_2 reduction experiments since they offer multiple advantages over other reactor designs discussed previously and can be combined with GDEs to further enhance mass transfer. Figure 10 shows a simplified scheme of a flow reactor used during CO2 reduction experiments.

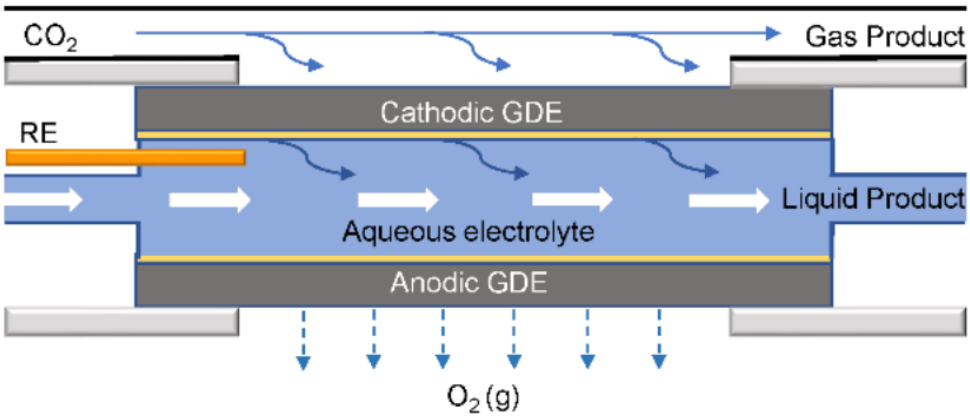

Figure 10 Schematic representation of a flow reactor with gas diffusion electrodes used in CO2 reduction experiments [35].

The first advantage is the ability to continuously operate the reactor, leading to relatively easy control of key parameters such as temperature, flow rate and CO_2 concentrations. This allows for quick assessments of different reaction conditions such as catalytic materials and electrolytes. Another advantage is their scalability. Due to the nature of continuously operated processes, it presents an ideal configuration for industrial, large scale CO_2 reduction processes.

However, the implementation of flow reactors for CO_2 reduction experiments also exhibits limitations. For example, the reactor design can induce mass transfer limitations due to poor mixing of the CO_2 containing electrolyte. To minimize these effects, careful consideration of the geometry of the reactor is often required to optimize flow patterns [36].

2.4 Photocatalyst selection and design

The selection and design of (photo-)catalysts is a crucial factor that greatly affects the overall efficiency, selectivity, and durability of the process. Different types of (photo-)catalysts have been successfully implemented in CO_2 reduction experiments. These include metals, metal oxides and metal-organic frameworks. When photocatalysts are used, the bandgap of the material significantly affects the efficiency of light absorption and conversion, which can result in efficient reduction processes.

2.4.1 Metallic and metal oxide (photo-)catalysts

Metallic photocatalysts often consist of single-component elements. The metallic oxide component can facilitate the absorption of light energy, the generation of electron-hole pairs and the transfer of electrons. This mechanism can create an electric field or potential that promotes activation and reduction of CO_2 and protons. Pure metallic catalysts are also implemented to act as electrocatalyst and can affect activation and reduction mechanisms of CO_2 [37].

Selection of the metallic or metal oxide component material has a significant effect on efficiency, selectivity, and stability. Commonly used semiconductor materials include TiO_2, ZnO and WO_3. TiO_2 is one of the most widely used semiconductor materials due to its excellent photocatalytic activity in the UV-range, low cost, and stability. ZnO is another commonly used semiconductor material for photoelectrochemical reduction of CO_2. It has a similar band structure to TiO_2 and can

also generate electron-hole pairs upon UV-irradiation. WO_3 is a promising semiconductor material due to its narrow bandgap and good stability [38]. It can be used for the electrochemical reduction of CO_2, although it may require additional doping or modification to enhance its catalytic activity.

On the other hand, commonly used metallic components include Pt, Au, Ag and Cu. Figure 11 gives a visual representation of different metallic components that have been implemented in electrochemical reduction experiments.

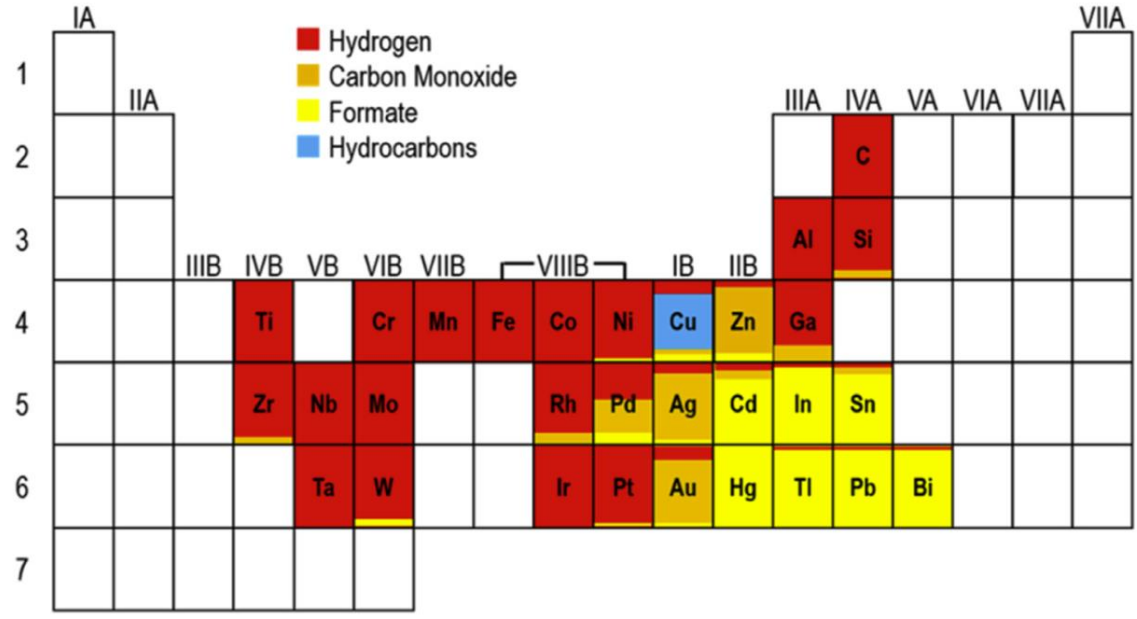

Figure 11 Periodic table depicting the selectivity of metallic electrocatalyst materials used in CO_2 reduction experiments [20]

It is noteworthy that Cu exhibits a high selectivity towards the production of hydrocarbons [21-24]. Other elements such as Cd, In or Sn show a high selectivity towards the production of formate [39-42]. Yet elements such as Fe, Ti, and Ni have a significant selectivity for hydrogen gas production [43-47].

In general, metallic catalysts do not have a bandgap that allows for light absorption and conversion, unlike semiconductor materials. To overcome this, bimetallic catalysts can be synthesized to obtain hybrid systems that have enhanced photocatalytic activity. Examples of this are Au or Ag that are deposited onto a metal oxide semiconductor [48-52]. These hybrid systems have shown improved charge transfer mechanisms and surface reactions. This is due to increased stability of the active catalytic reaction sites. However, various factors can affect the performance of metallic photocatalysts, including light intensity and wavelength, temperature, and pH. The assessment of optimal reaction environment is thus crucial for achieving efficient, selective, and stable CO_2 reduction.

2.4.2 Metal-organic framework (photo-)catalysts

Metal-organic framework (MOF) (photo-)electrocatalysts have been recently developed and implemented in electrochemical reduction of CO_2. MOF (photo-)electrocatalysts are porous crystalline materials consisting of metal ions linked by organic ligands. They have the unique

quality of being tuneable to specific properties. Furthermore, the porosity of MOF materials offers a high specific surface area [53,55].

Multiple MOF materials have demonstrated electrocatalytic activity during CO_2 reduction experiments. A prominent example are copper-based MOF electrocatalysts as they exhibit high electrocatalytic activity and selectivity [54]. Additionally, several MOF materials exhibit photocatalytic abilities under light irradiation. For example, a zirconia-based MOF, namely UiO66, showed an enhanced photocatalytic activity towards CO2 reduction under both visual and ultraviolet irradiation, due to its unique band structure and defect sites [56].
Current research aims to further improve the (photo-)electrocatalytic activity of MOF materials through the integration of functional components such as metal nanoparticles, conductive polymers, or other co-catalysts [57].

2.4.3 Strategies to enhance (photo-)catalytic performance

The enhancements of photocatalysts for CO_2 reduction can be achieved through several strategies. One approach involves the addition of co-catalysts onto the catalyst surface to facilitate increased charge transfer. Specifically, this can be achieved through the addition of noble metal nanoparticles such as Pt or Au. The noble metal coating allows for an enhanced activity through the promotion of the separation of electron-hole pairs. It was concluded that this was likely caused by multiple factors such as increased conductivity and increased CO_2 adsorption [58]. Furthermore, the addition of molecular co-catalysts can also promote the efficiency of a catalytic reaction. For example, cobalt phthalocyanine has been successfully implemented onto a titanium oxide photocatalyst and resulted in an increased CO_2 reduction activity and selectivity towards ethanol [59].

Morphological modification represents another effective strategy for enhancing the performance of photoelectrocatalysts. The morphology has a significant effect on the surface area of the photoelectrocatalysts. This in turn significantly influences the number of active CO_2 reduction sites. Morphological modification can result in high specific surface area [60]. Additionally, the incorporation of defects within the photocatalytic structure can create a further increase of catalytic activity and selectivity. An example of this is the presence of oxygen vacancies on a TiO_2 surface. This has been shown to promote an efficient electron-hole pair separation which directly resulted in further enhanced activity and selectivity [61]. To achieve efficient morphological modifications, several techniques have been developed. These include hydrothermal synthesis [62], solvothermal synthesis [63,64] and template assisted synthesis [65,66].

Doping, which involves the introduction of foreign atoms into photocatalyst materials, represents a third strategy to enhance photocatalytic performance [67,68]. Doping can be achieved through multiple techniques, such as co-precipitation [69] and solid-state reaction [70]. Commonly used dopants are metal ions, non-metal ions and transition-metal ions. The metal ions are commonly used as dopants because they exhibit a high electron affinity and electron trapping capacity which leads to improved charge separation and transfer [71]. Examples of metal ions are Cu, Ag, Pt and Pd. Non-metal ions, on the other hand, can also be implemented due to their ability to modify the energy states in the bandgap. Usually it narrows the bandgap, resulting in broader absorption spectra [72]. This is especially applicable for energy harvesting of the solar spectrum. Additionally, transition-metal ions such as Fe, Ni or Co can also change the bandgap structures of the photocatalyst by introducing new energy levels [73]. Doping efficiency depends primarily on the

concentration, size, and spatial arrangements of the dopant. The optimal concentration varies according to photocatalytic material that is used [74].

A more recent implementation, namely nanostructuring, has also been employed to enhance the catalytic activity. Nanostructuring of photocatalysts can significantly increase the surface area of the photocatalyst, resulting in increased reaction rates, efficiency, and selectivity [75]. Nanostructuring can be achieved through techniques such as sol-gel, hydrothermal and electrospinning methods to influence the size and shape of nanoparticles on the photocatalyst surface [76].

3. Materials and methods

This section outlines the materials and methods employed during the optimization studies. The description includes details regarding the reactor setup, experimental procedures, and analytical techniques utilized to investigate the various parameters. The materials utilized in the experiments, such as electrocatalysts, electrolytes, and instruments are introduced, along with the experimental procedures.

3.1 Optimization of reactor configuration

3.1.1. Initial reactor configuration

The initial reactor design consists of an 'H-type' reactor. An oxidized copper plate measuring 4,0 cm by 2,5 cm is implemented as a cathodic and a TiO_2 (thickness = 150 nm) layer deposited on fluorine-doped tin oxide (FTO) as an anodic electrocatalyst respectively. The cathodic and anodic compartments are separated by a Nafion™ membrane. Additionally, an Ag/AgCl reference electrode is installed in the cathodic compartment. The spacing between the copper and reference electrodes is ca. 0,7 cm. All three electrodes are connected to a potentiostat/galvanostat (Autolab PGSTAT30), which regulates an applied external potential to the cathodic and anodic compartments. Figure 12 gives a visual representation of the initial reactor setup.

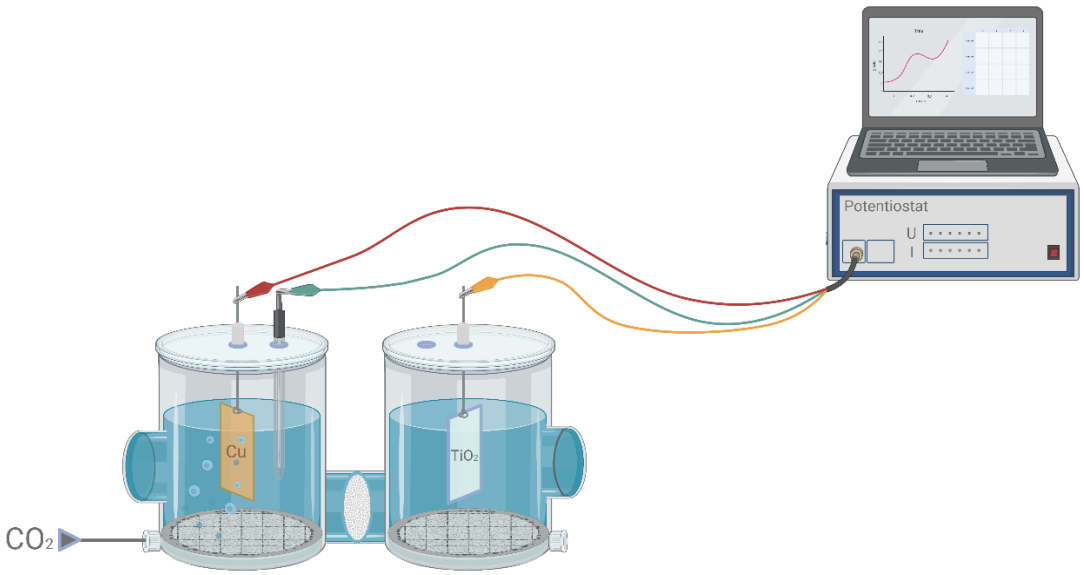

Figure 12 Initial reactor configuration.

3.1.2. Optimized reactor configuration

In addition to the initial reactor configuration described in 3.1.1, an external recycle is now implemented on both the cathodic and anodic sides using peristaltic pumps. Furthermore, external CO_2 dissolution is implemented. To achieve an efficient CO_2 dissolution, a diffuser was attached to the incoming CO_2 duct. The electrocatalyst configuration was also changed. The cathodic electrocatalyst consists of a commercial grade, metallic copper wire with a diameter of 0,1 cm and a length of 15,71 cm. The copper wire is prepared by scrubbing with sandpaper. The anodic electrocatalyst consists of a platinum wire with a diameter of 0,1 cm and a length of 15,71 cm. Figure 13 provides a schematic overview of the reactor configuration.

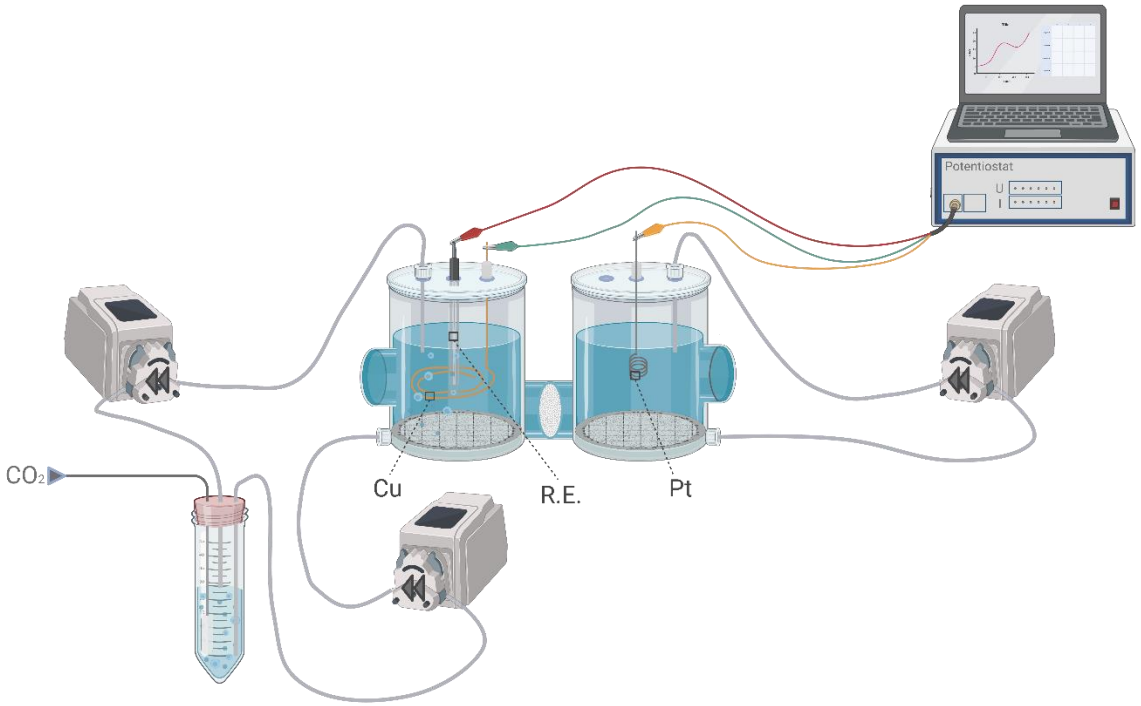

Figure 13 Reactor configuration with external recycles and CO_2 dissolution.

3.1.3. Reaction conditions

Experiments are conducted by adding 45 ml of a 0,1 M Na_2SO_4 (VWR Chemicals) electrolyte solution to the cathodic and anodic compartments respectively. Additionally, 35 ml is also added to the CO_2-dissolution container. Before the start of the experiment, the saturation of pressurized CO_2 is started in the external dissolution compartment. The saturation is maintained for 30 min at 91,8 ml/min. The reaction is then started by applying an external potential of -2V (vs Ag/AgCl) through the potentiostat. The reaction time varies between 0,5 – 12 hrs.

3.1.4. Analysis techniques

After each experiment a sample is taken from the cathodic compartment and subsequently analyzed by the headspace gas chromatograph coupled with mass spectrometry (GC-MS) for hydrocarbons.

3.2 Optimization of external potential

3.2.1. Reactor configuration

The reactor configuration discussed in 3.1.2 is expanded by adding a H_2 and CO meter (Honeywell BW Solo). These are directly connected to the headspace above the catholyte in-line analysis of H_2 and CO concentrations. Furthermore, a pressurized N_2 duct was added. Figure 14 shows a schematical representation of the reactor configuration.

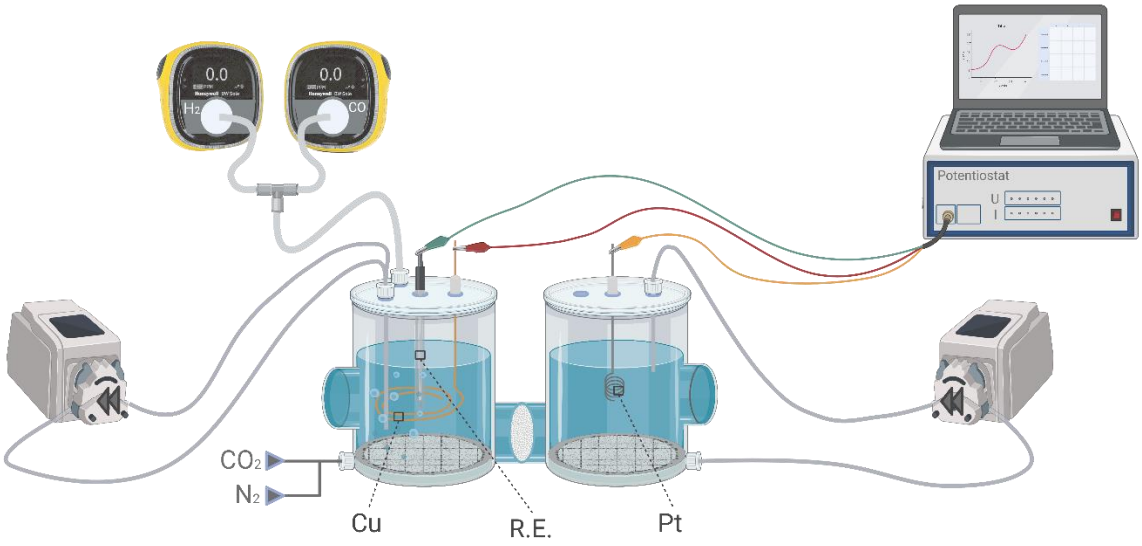

Figure 14 Reactor configuration with internal CO_2 dissolution and in-line H_2/CO measurements

3.2.2. Experimental procedure

Experiments are conducted by adding 45 ml of a 0,1 M Na_2CO_3/$NaHCO_3$ (Merck) electrolyte solution to both cathodic and anodic compartments. The catholyte is first saturated with pressurized N_2 or CO_2 for 30 min at 91,8 ml/min. Subsequently, the reaction is started by applying varying external potentials, ranging between -1 V to -2 V in segments of -0,2 V (vs Ag/AgCl). The reaction time is set to 1 hr.

3.2.3. Sample analysis techniques

Experiments are conducted with N_2 and CO_2 saturation separately. chrono amperometry measurement data is collected by the potentiostat. The average current is calculated by averaging the current measurement between 3000 s and 3600 s. Simultaneously, the H_2 and CO concentrations of the cathodic gas phase are manually collected throughout the experiment. Additionally, a catholyte sample was extracted after each experiment for hydrocarbon analysis on the GC-MS.

3.3 Optimization of electrolyte selection

3.3.1. Reactor configuration

To further optimize film diffusion at the electrocatalyst surfaces, the external recycles are replaced with a magnetic stirrer. Figure 15 gives a schematic overview of the reactor configuration.

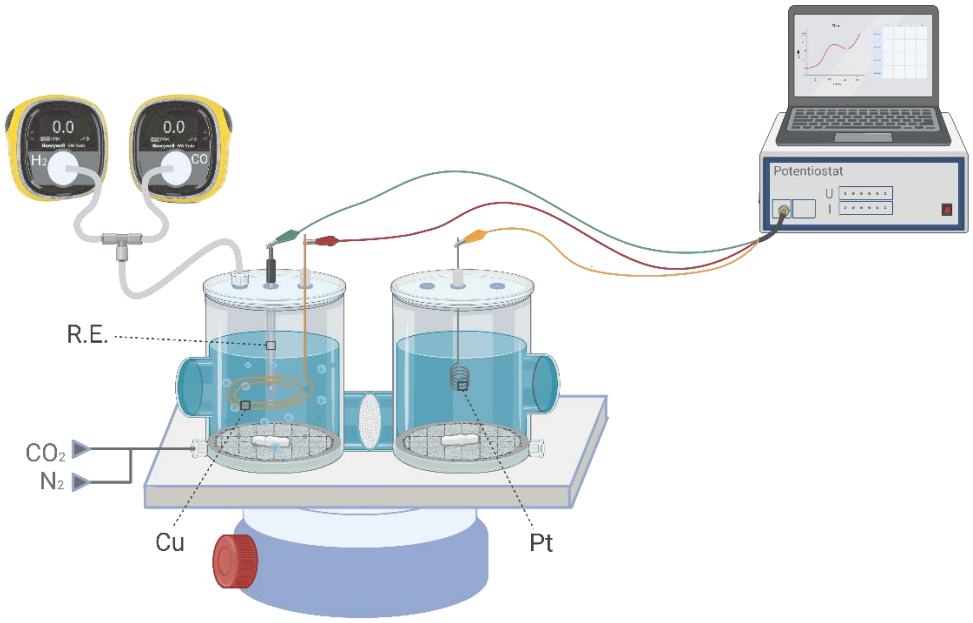

Figure 15 Reactor configuration with magnetic stirrer.

3.3.2. Reaction conditions

Experiments are conducted by adding 45 ml of a 0,1 M KI (Merck), KI+Na_2CO_3/$NaHCO_3$, Na_2CO_3/$NaHCO_3$ (Merck), or Na_2SO_4 (VWR chemicals) solution to the cathodic and anodic compartments. Before the start of the reaction, the catholyte is saturated with pressurized N_2 for 30 min at a flowrate of 91,8 ml/min. Thereafter, the reaction is started by applying an external potential of -1 V (vs Ag/AgCl). During the first 1000 s of the reaction, N_2 saturation is maintained at a flow rate of 20,3 ml/min. Subsequently, the N_2 saturation is terminated, while pressurized CO_2 is now supplied to the catholyte. The CO_2 dissolution is maintained for 2600 s with a flow rate of 20,3 ml/min.

3.3.3. Analysis techniques

N_2 and CO_2 saturation are implemented in the same experiment to assess the CO_2 dissolution effects more accurately. Chrono amperometry measurement data is collected in triplicate for each electrolyte. The average current during N_2 and CO_2 saturation is calculated by averaging the current between 400-1000 s and 3000-3600 s respectively. Additionally, H_2/CO concentration measurement data are collected. After each experiment, a catholyte sample is analyzed through GC-MS.

3.4 Optimization of TiO_2 catalyst loading

3.4.1. Reactor configuration

The reactor setup is modified to accommodate for a UV-irradiation source. Figure 16 gives a schematical representation of the reactor setup. The anodic electrocatalyst consists of a TiO_2 layer deposited on conductive glass with varying thickness. Four thicknesses were analyzed, namely 150nm, 370nm, 690nm. Figure 16 provides a schematic representation of the reactor configuration.

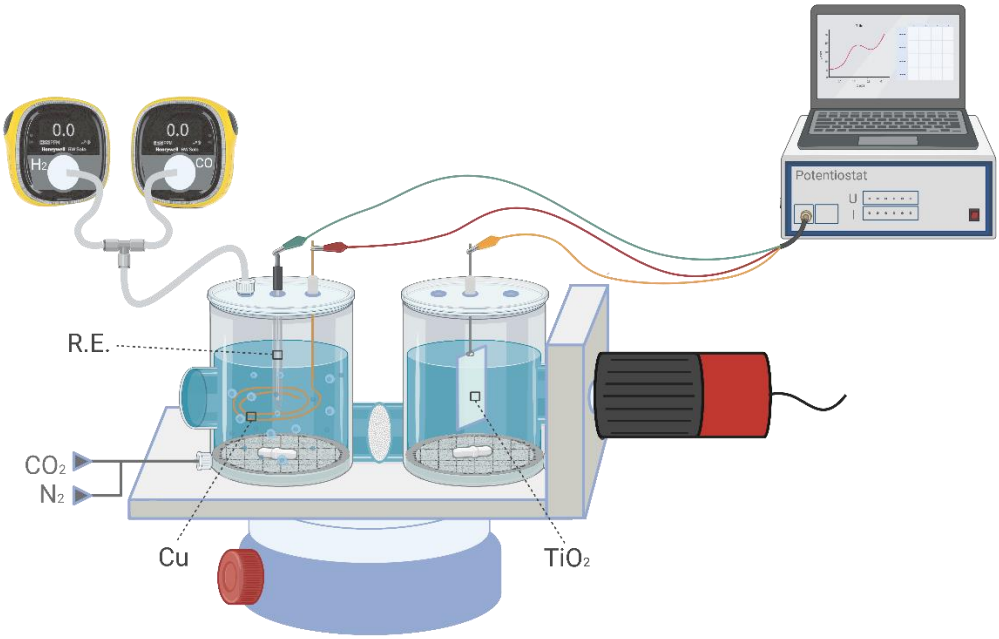

Figure 16 Reactor configuration with UV-irradiation of TiO_2 electrocatalyst.

3.4.2. Reaction conditions

Experiments are conducted by adding 45 ml of 0,1 M KI electrolyte to both cathodic and anodic compartments Initially, the catholyte is saturated with pressurized N_2 for 30 min at a flowrate of 91,8 ml/min. Subsequently, the reaction is started by applying an external potential of -1 V (vs Ag/AgCl). During the first 1000 s of the reaction, N_2 saturation is maintained at a flow rate of 20,3 ml/min. Thereafter, the N_2 saturation is terminated, while pressurized CO_2 is now supplied to the catholyte. The CO_2 dissolution is maintained for 2600 s with a flow rate of 20,3 ml/min.

3.5.3. Analysis techniques

Three replicate chronoamperometry measurements are conducted for each electrolyte. The average current during N_2 and CO_2 saturation is determined by averaging the current within the time intervals of 400-1000 s and 3000-3600 s, respectively. Furthermore, measurements of H_2/CO concentrations are collected. Following each experiment, a sample of the catholyte is analyzed using GC-MS.

4. Results and discussion

This section presents the results and discussion regarding the optimization studies. The research focusses on multiple parameters including film diffusion, CO_2 dissolution, electrocatalyst configuration, external potential, electrolyte selection, TiO_2 electrocatalyst configuration, and understanding of reaction mechanics and products through cyclic voltammetry and pH analysis. These results are discussed chronologically and provide crucial insights into the effects of these parameters on the efficiency, selectivity, and performance of the electrochemical processes.

4.1 Optimization of reactor configuration

In this section, an investigation regarding film diffusion, CO_2 dissolution, and electrocatalyst configuration was conducted to improve the current density and current stability.

To enhance film diffusion and dissolved CO_2 concentrations, external recycles were implemented to both cathodic and anodic compartments using peristaltic pumps. This modification was intended to improve mixing and mass transfer at the electrocatalyst surfaces. Additionally, pressurized CO_2 was externally dissolved to increase CO_2 saturation levels. As a result of the pulsating effect of the peristaltic pumps, the current readings on the potentiostat were relatively unstable. To improve this, the electrocatalyst configuration was optimized. The cathodic electrocatalyst was changed from a rectangular, oxidized copper plate to a metallic copper wire. The anodic catalyst was changed from a TiO_2 layer deposited onto conductive glass to a platinum wire. Figure 17 shows the chrono amperometry measurements for the initial and optimized reactor design.

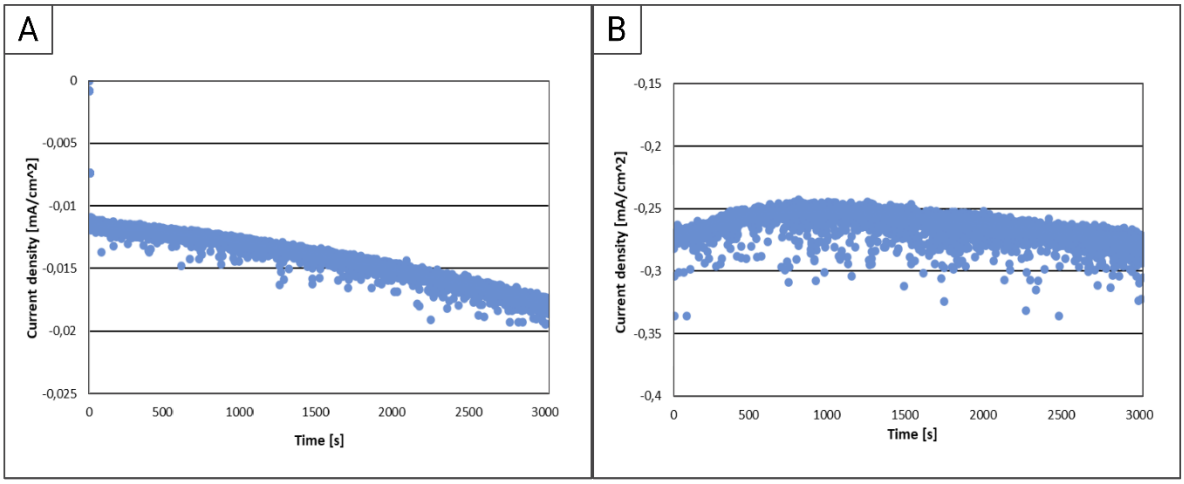

Figure 17 Chrono amperometry measurements: (A) Initial reactor configuration; (B) Optimized reactor configuration

The optimization of film diffusion, CO_2 dissolution, and electrocatalyst configuration resulted in improved average current density, increasing from -1,4 $\mu A/cm^2$ for the initial reactor design to $-2{,}6*10^2$ $\mu A/cm^2$ for the optimized design. Additionally, the stability of the current readings for the optimized reactor design also improved significantly. Furthermore, liquid phase samples of the catholyte were analyzed by GC-MS to identify and quantify hydrocarbon products. However, no hydrocarbons were detected. It was assumed that hydrocarbon concentrations remained below the sensitivity limit of the GC-MS. The external CO_2 dissolution was consequently removed in favour of in-reactor dissolution due to the extra cathodic reactor volume it introduced. This would cause a dilution of any liquid phase reaction products, including hydrocarbons.

4.2 Optimization of external potential

This section investigates the effects of different external potentials on the current density. Additionally, H_2 and CO sensors were introduced to the headspace of the cathodic compartment to identify the optimal external potential with maximum selectivity towards CO formation. The reactor setup, including potentiostat, external recycles, and H_2 and CO sensors, was operated at external potentials at -1 V, -1,2 V, -1,4 V, -1,6 V, -1,8 V, and -2 V (vs Ag/AgCl). The current was measured for each external potential through the potentiostat using chrono amperometry readings. Additionally, an N_2 saturation experiment was conducted to serve as a reference for comparison to CO_2 saturation experiment at each external potential. All experiments were conducted in triplicate. Once the reaction was terminated, GC-MS analysis was conducted on catholyte samples after a reaction time of 1 h.

Firstly, the chrono amperometry readings provided valuable information on the current density as a function of time and external potential. These measurements allowed for the characterization of the electrochemical response under various voltage conditions. By analyzing the obtained current profiles, it was possible to assess the effects of the external potential on the kinetics of the electrochemical process. However, high deviations between experiments were observed. For this reason, it was not possible to determine reliable differences between N_2 and CO_2 saturation experiments at given external potential. As a result, only the average current density of the CO_2 saturation experiments is discussed. The chronoamperometry data, showcasing the time-dependent current measurements, has been provided in Appendix A for reference and further analysis. Figure 18 shows the average current density of the CO_2 saturation experiments in function of the external potential.

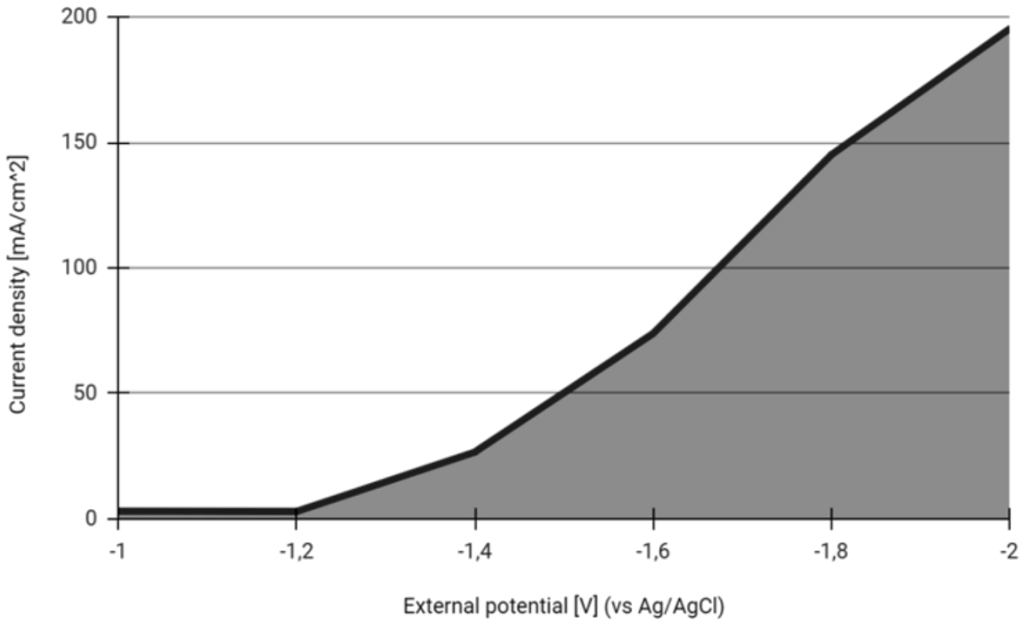

Figure 18 External potential effect on the current density relative to the cathodic electrocatalyst

The current density is relatively low at ca. 3 mA/cm^2 for external potentials of -1 V and -1,2 V (vs Ag/AgCl). At higher potentials (≥ -1,4 V), the current density increases significantly. Possible explanations are increased H_2, CO and hydrocarbon production with higher external potentials.

The increased external potential leads to a corresponding increase in the kinetics of each reaction, thus contributing to the observed trend.

Secondly, to further characterize the effects of external potential on the selectivity of gaseous reaction products, the production of H_2 and CO was monitored during the experiments. However, at external potentials of -1,8 V and -2 V (vs Ag/AgCl), the upper sensitivity limit was exceeded for both the H_2 and CO sensors. Thus, selectivity data is only available for external potentials ranging between -1 V and -1,6 V (vs Ag/AgCl). Figure 19 shows the relative concentrations of H_2 and CO in function of the external potential, ranging from -1 V to -1,6 V (vs Ag/AgCl).

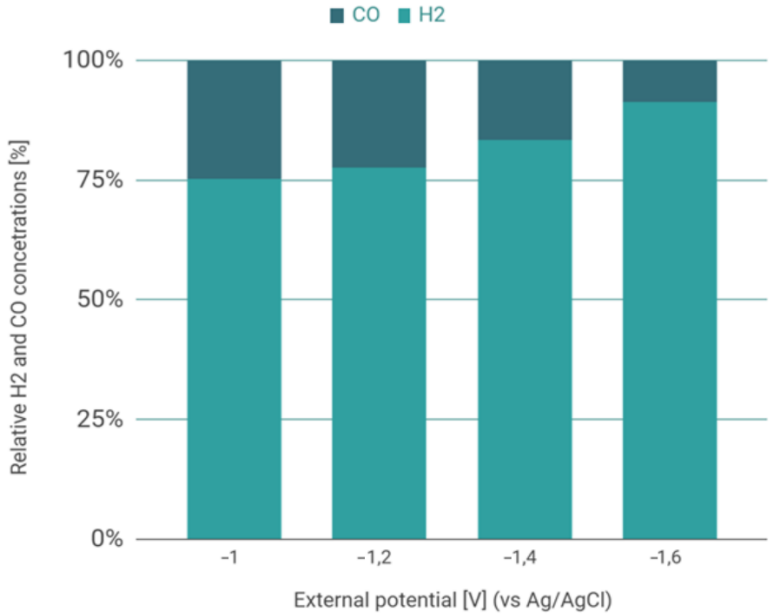

Figure 19 External potential effect on the relative H_2 and CO concentrations.

This data shows that the selectivity towards CO formation diminishes with increasing potential. The highest CO selectivity was reached at the lowest potential of -1 V (vs Ag/AgCl). Additionally, it can be inferred that higher external potentials induce a higher selectivity towards H_2. This trend is likely caused by CO_2-mass transfer limitations at the cathode surface, resulting in decreased CO production.

Lastly, catholyte samples were extracted after each experiment. These were analyzed by GC-MS for liquid phase hydrocarbon detection. Although no hydrocarbons were detected, it was still assumed that this is likely due to low concentrations for which the sensitivity of the analysis method was not sufficient.

To optimize further experimental studies within this research, future experiments will be conducted at an external potential of -1 V (vs Ag/AgCl) to maximize CO production. Additionally, further experiments will be conducted with N_2 and CO_2 saturation consecutively within the same experiment. This method is expected to enable a direct comparison between these two conditions, effectively reducing the uncertainties associated with separate experiments. Moreover, it was also concluded that the use of external recycling negatively impacted the current measurements. This is due to the pulsating nature of the peristaltic pumps, which in turn caused a pulsating effect on the grade of mixing inside the reactor compartments. Consequently, the external recycles were substituted for magnetic stirrers. It is expected that this will further increase the intensity of mixing which in turn could positively impact film diffusion at the catalyst surfaces.

4.3 Optimization of electrolyte material

In this section, four different electrolytes were analyzed to evaluate their effects on the electrochemical reactions. Specifically, KI, KI+Na_2CO_3/$NaHCO_3$, Na_2CO_3/$NaHCO_3$, and Na_2SO_4 were investigated. The choice of electrolyte played a crucial role in determining the performance of the electrochemical system. The different electrolytes provided varying ionic conductivity and pH conditions, which affected the reaction kinetics and product selectivity. Additionally, the degree of mixing was optimized. This was achieved through replacement of external recycles with magnetic stirrers. This change was implemented to further enhance film diffusion, ensuring efficient mass transport within the reactor.

Chrono amperometry experiments were conducted with N_2 and CO_2 saturation consecutively within the same experiment. This allowed for the evaluation of the carbon reduction current or the current increase resulting from CO_2 dissolution compared to N_2 dissolution. For reference, the chronoamperometry data can be found in Appendix B. Figure 20 illustrates a typical chrono amperometry experiment for the KI, KI+Na_2CO_3/$NaHCO_3$, and Na_2CO_3/$NaHCO_3$ electrolytes.

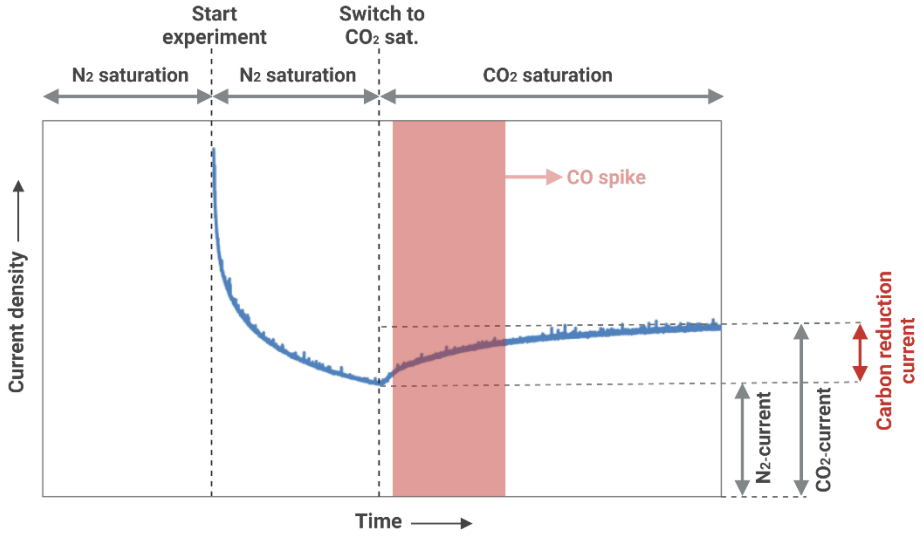

Figure 20 Example of a typical chrono amperometry experiment, including saturation procedure and effects on the resulting current.

Before the experiment starts, an N_2 saturation is maintained for 30min. Then, an external potential is applied to start the reaction. This induces a high current at first, which gradually decreases and stabilizes. This behaviour is likely caused by multiple factors. Firstly, the reduction of residual amounts of O_2 to H_2O at the cathode can offer a partial explanation. Secondly, it is also suspected that a decrease in current can be caused by the onset of film diffusion limitations at the electrocatalyst surfaces. Lastly, a high initial current can also be caused through the polarization in acidity of the cathodic and anodic compartments respectively. However, continuous pH measurement data is required to confirm this.

Consequently, the N_2 saturation is terminated while the CO_2 saturation is initiated. This induced a significant increase in reduction current for all experiments. The current increase is referred to as the carbon reduction current. The onset of the carbon reduction current also coincided with a spike in CO production for KI, KI+Na_2CO_3/$NaHCO_3$, and Na_2CO_3/$NaHCO_3$ electrolytes. The formation of CO generally starts 4 min after the CO_2 saturation is activated and lasts for 10 min. Once the CO production has decreased to zero, a further decrease in current can be observed. A possible

explanation for this behaviour is that CO is an intermediate product in the carbon reduction chain. It is also suspected that the pH steadily decreases during the CO_2 saturation, further increasing the proton concentration in the catholyte. This could then act as a driving force for further reduction of CO to hydrocarbons, effectively decreasing the selectivity towards CO as the reactions continue. This would also explain why the current increases after CO production has ceased.

Furthermore, it is noteworthy to mention that the experiments with Na_2SO_4 yielded a similar carbon reduction current response. Yet, no CO formation spike was detected. However, a steadily increasing amount of H_2 production was observed throughout the remainder of the experiments. This is likely caused by the relatively low initial pH of this electrolyte, which is significantly lower than the other three electrolyte solutions. A lower pH is known to increase selectivity towards H_2 formation due to the relatively low activation energy of the HER in these conditions [17,77].

To select the most efficient electrolyte, the average current during CO_2 saturation was calculated. Figure 21 gives a visual overview of the results for each electrolyte.

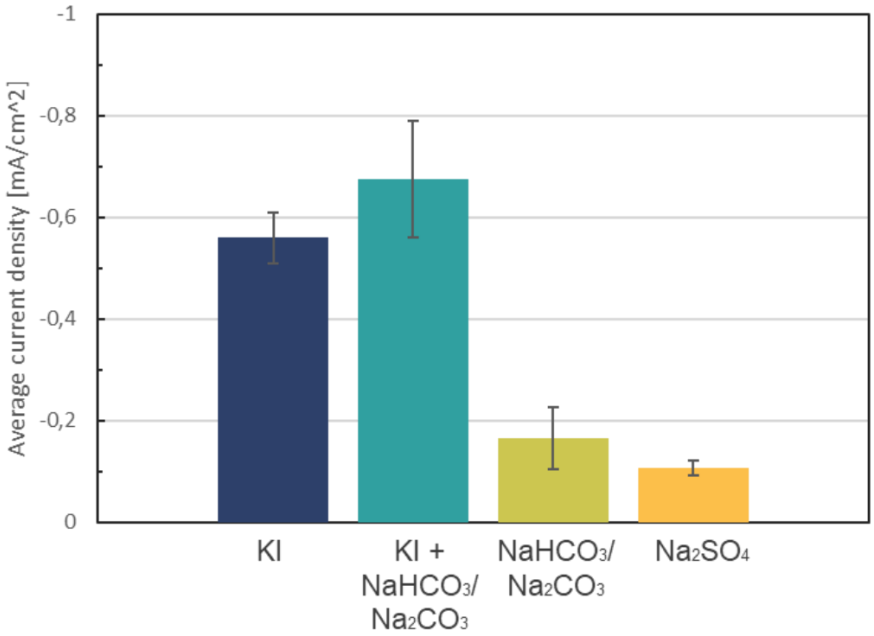

Figure 21 Average current during CO_2 saturation.

The highest average current was observed for KI+Na_2CO_3/$NaHCO_3$, at ca. -3,4 mA. While the lowest average current was observed for Na_2SO_4 at -0,52 mA. Notably, the Na_2CO_3/$NaHCO_3$ electrolyte also showed relatively low currents during CO_2 saturation. In general, electrolytes containing KI showed a significant increase in average current. This is likely due to the high ionic conductivity that KI facilitates.

To further analyse the relative response to CO_2 saturation, the carbon reduction current (or current increase) was calculated. Figure 22 illustrates these results.

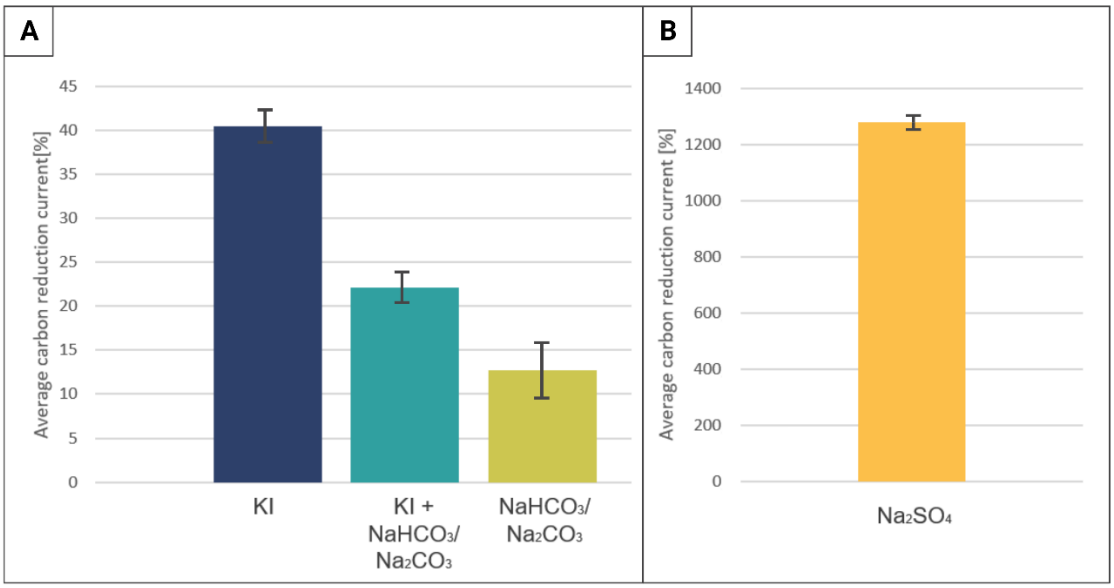

Figure 22 Average carbon reduction current: (A) KI, KI + $NaHCO_3/Na_2CO_3$, and $NaHCO_3/Na_2CO_3$; (B) Na_2SO_4

The highest current increase of ca. 1250% was observed for Na_2SO_4. Again, this is likely caused by the increased H_2 formation due to a high initial acidity of the electrolyte, which increases the selectivity towards H_2. Additionally, KI, KI+Na_2CO_3/$NaHCO_3$, and Na_2CO_3/$NaHCO_3$ also showed a carbon reduction current, although these are significantly lower compared to Na_2SO_4. Here, KI exhibited the highest carbon reduction current at ca. 40 %, while KI+Na_2CO_3/$NaHCO_3$ and Na_2CO_3/$NaHCO_3$ showed an increase of ca. 22 % and 12,5 % respectively. Once again, this behaviour can be ascribed to the increased ionic conductivity that KI enables. Furthermore, KI+Na_2CO_3/$NaHCO_3$ and Na_2CO_3/$NaHCO_3$ are not ideal for the assessment of carbon reduction currents due to the presence of reactive carbonates anions in the electrolyte. This can affect the carbon reduction kinetics, resulting in poor comparability to the KI electrolyte.

To thoroughly compare the electrolytes and select the optimal electrolyte, the average current, carbon reduction current, current stability, pH, and CO/H_2 selectivity are compared in table 1.

Table 1 Overview of electrolyte characteristics detailing average current, average current increase, current stability, pH, and CO/H2 selectivity.

	KI	**KI + $NaHCO_3/Na_2CO_3$**	**$NaHCO_3/Na_2CO_3$**	**Na_2SO_4**
Average current density	*High*	*High*	*Medium*	*Low*
Average carbon reduction current	*Medium*	*Low*	*Low*	*High*
Current stability	*Stable*	*Stable*	*Unstable*	*Stable*
pH	*7*	*9*	*9,5*	*6*
CO/H_2 selectivity	*CO*	*CO*	*CO*	*H_2*

Since a selectivity towards CO_2 reduction is desired, Na_2SO_4 is least effective due to its selectivity towards H_2 formation. Also, the electrolytes natively containing carbonate anions are not desired since it introduces uncertainty regarding carbon reduction current, as mentioned before. Conclusively, KI is selected as the optimal electrolyte for analytical purposes regarding direct CO_2 reduction.

It is also noteworthy that catholyte samples were analyzed for hydrocarbon products through GC-MS analysis, but no hydrocarbons were detected. Yet, in another attempt to assess the presence of hydrocarbon reaction products, FTIR analysis was conducted. Here the catholyte samples before and after the experiments were analyzed and compared. However, no significant changes in absorption peaks were observed.

4.4 Optimization of TiO_2 catalyst loading

In this section, the effects of TiO_2 catalyst thickness on the electrocatalyst loading are examined. The goal was to determine the optimal thickness by assessing the impact on chronoamperometry readings obtained using a potentiostat. Additionally, the influence of UV-irradiation on the TiO_2 surfaces and resulting current readings was investigated using a UV lamp. Surprisingly, it was found that UV light had no effect on the resulting current. Therefore, subsequent chronoamperometry experiments were conducted without UV light. The results of these measurements are provided in Annex C for further reference. Despite TiO_2 being a semiconductor acting as an insulator, noticeable differences in resulting current were observed for different TiO_2 catalyst loadings.

The TiO_2 catalyst thicknesses analyzed in this study were 150 nm, 370 nm, and 690 nm. The average catalyst loading for each thickness was found to be 18%, 24%, and 67% respectively. Figure 23 shows the catalyst loading increase for each TiO_2 catalyst thickness.

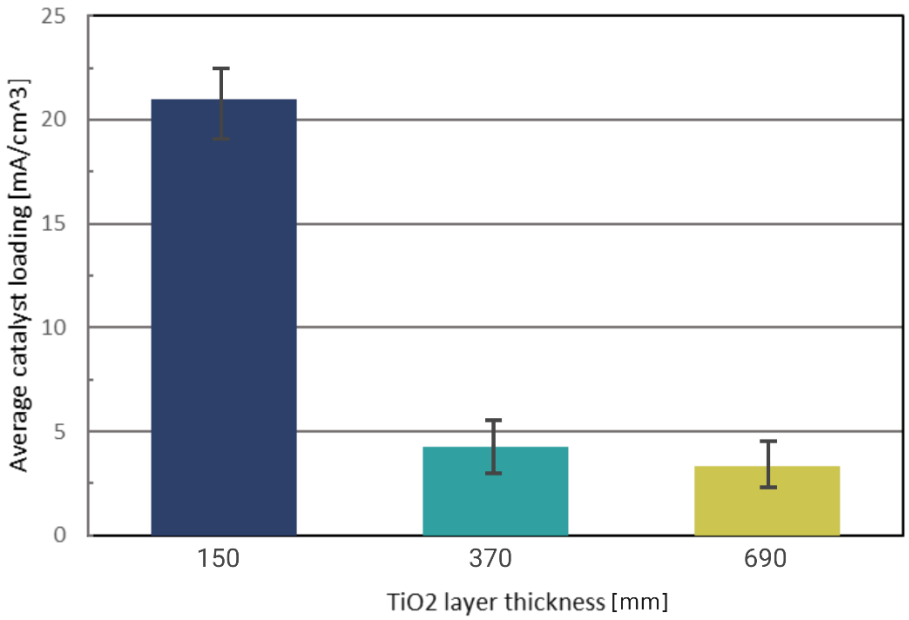

Figure 23 Average catalyst loading for varying TiO_2 layer thickness.

These results indicate a significant effect of the resulting current on the TiO_2 catalyst loading. The highest catalyst loading was obtained for a TiO_2 catalyst thickness of 150 nm, indicating the optimal thickness range within the tested range. Nevertheless, it is observed that the catalyst loading decreases as the catalyst thickness further increases. This decrease can be attributed to multiple factors, such as morphological differences, charge transport, and interfacial properties, which vary with TiO_2 catalyst thickness. An additional explanation can be found in the effect of catalyst thickness on pore diffusion efficiency. When a catalyst layer is too thick, it can lead to limitations in pore diffusion, affecting the overall performance of the catalytic system. In a thin catalyst layer, reactants can easily access the active sites, and products can quickly diffuse away, resulting in efficient reaction kinetics. However, as the catalyst thickness increases, the diffusion path length for the reactants and products also increases. This longer path length can lead to slower diffusion rates and higher mass transport resistances. Additionally, this can also result in electron-hole recombination, effectively decreasing the overall efficiency of the oxidation reactions. Figure 24 provides a visual representation of the effect of catalyst thickness on pore diffusion.

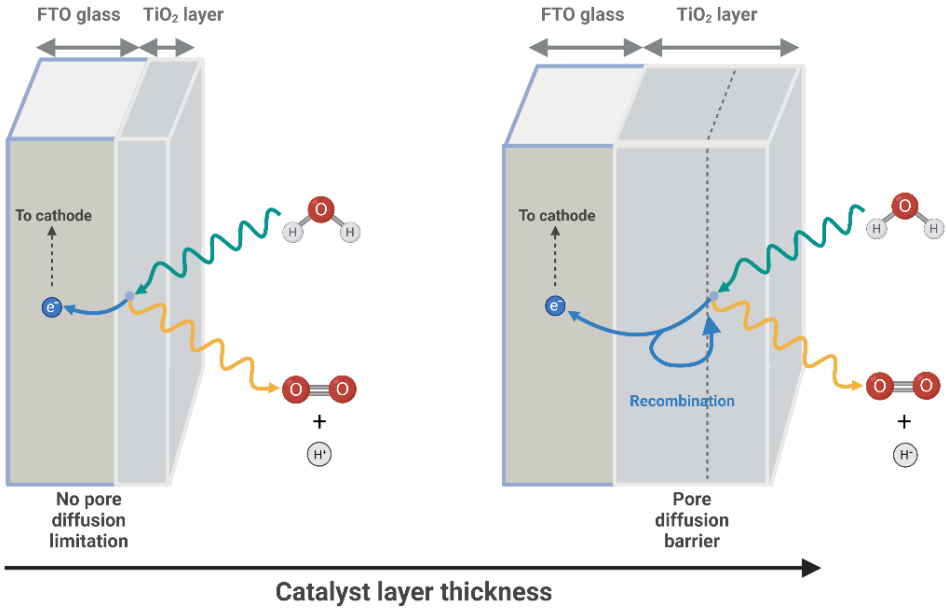

Figure 24 TiO_2 catalyst layer thickness effect on pore diffusion properties.

In general, the thickness of the TiO_2 can significantly affect the overall performance by maximizing the current response and facilitating efficient charge transfer processes. Conclusively, further characterization and analysis is recommended. Specifically, surface and microstructural investigations could provide additional insights into the underlying mechanisms responsible for the observed trends in current response with varying TiO_2 catalyst loading.

Additional GC-MS analyses were conducted on the catholyte samples but revealed no detection of hydrocarbon products. Despite analyzing different TiO_2 layer thicknesses and UV-irradiation, no evidence of hydrocarbon formation was observed. These findings indicate that under the experimental conditions and TiO_2 configurations studied, the electrochemical reactions did not generate significant amounts of hydrocarbons.

4.5 Analysis of reaction mechanisms and conditions

Chrono amperometry and pH measurements are discussed in this section to evaluate the effect of pH during CO_2 dissolution. When analyzing the pH measurements obtained during chrono amperometry experiments, several noteworthy observations emerge. Throughout the experiment, distinct pH variations were observed in both cathodic and anodic compartments. Figure 25 shows the current profile and pH measurements obtained during a chrono amperometry experiment.

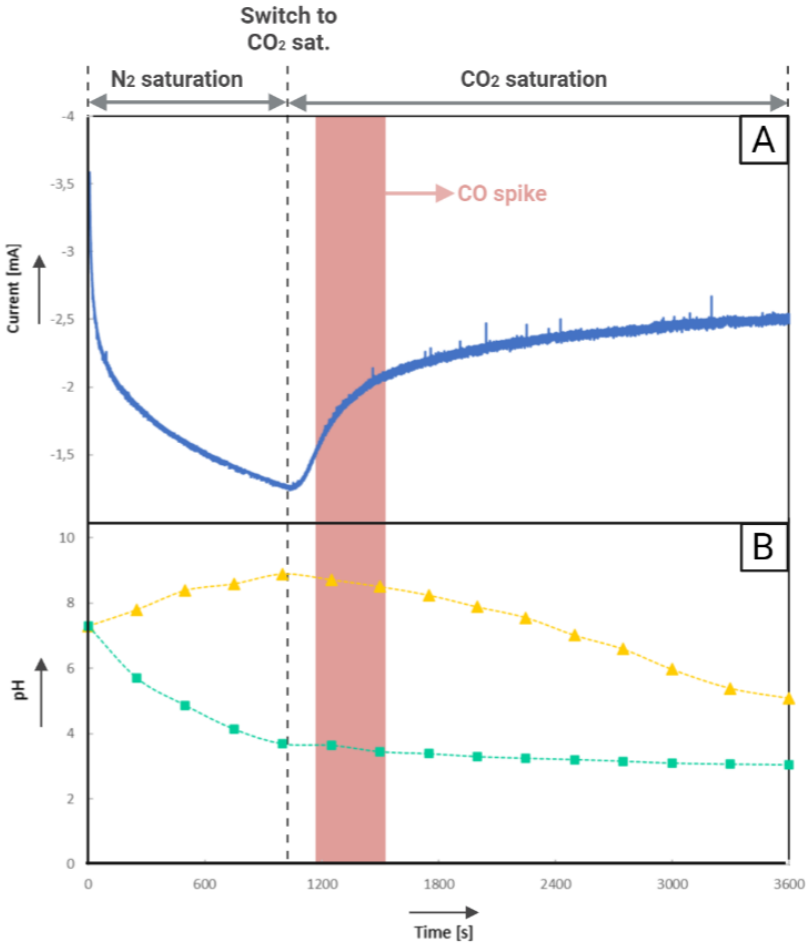

Figure 25 Chrono amperometry analysis results: (A) Current profile; (B) Corresponding pH measurements

At the start of the experiment (time = 0s), both the cathode and anode exhibited a pH of 7,31, indicating a neutral environment. During the N_2 saturation, the pH at the cathode gradually increased and reached a maximum value of 8,9 at 1000 s. This rise in pH can be attributed to factors other than the reduction of CO_2, as no dissolved CO_2 was present in the catholyte during this period. Potential explanations for this pH increase could involve the reduction of residual O_2 to H_2O at the cathode or other electrochemical reactions occurring in the system. Moreover, the disparity in acidity between the cathode and anode compartments could influence the current behaviour. The initial high current observed might be attributed to the polarization in acidity.

In contrast, the pH at the anode displayed a significant increase during N_2 saturation. The pH decreased from the initial value of 7,31 to a minimum of 3,05 at 3600 s, indicating the accumulation of protons in the anodic compartment. This acidification is likely attributable to oxidation reactions at the anode, leading to the generation of protons through water decomposition.

During CO_2 saturation (t = 1000-3600 s), a significant increase in current is observed. This finding aligns with the decreasing pH trend in the cathodic compartment. Additionally, the pH in the anodic compartment stabilized within this timeframe. This behaviour can be attributed to the formation of hydrocarbons. Since this would imply proton consumption in the cathodic compartment, protons from the anode can now migrate to the cathode. As a result, the anodic acidity stops decreasing and then stabilizes. Furthermore, a CO formation spike was observed during CO_2 saturation between 1200-2000 s. The fact that the current is still increasing when CO production ceases, can indicate that CO is an intermediate product. Once the acidity reaches a sufficient level, CO can theoretically undergo further reduction to form hydrocarbon products. An additional explanation for the current increase can be found through H_2 formation since it is also highly dependent on the acidity of the catholyte. However, no H_2 formation was detected by the H_2 sensor. This was confirmed through in-line GC-FID analysis.

Conclusively, the pH measurements provided valuable insights regarding the chrono amperometry results. Further research is recommended to gain a better understanding of the kinetics and selectivity of CO conversion pathways. Understanding the relationships between pH variations and current behaviour is crucial for advancing the understanding and optimization of electrochemical CO_2 reduction processes.

5. Conclusion and future projections

This research aimed to optimize the electrochemical reduction of CO_2 for enhanced CO and hydrocarbon production. Throughout the investigation, various parameters were examined in order to increase the concentration of CO_2 reduction products in the catholyte. These included mixing, CO_2 dissolution, electrocatalyst configuration, external potential, electrolyte selection and pH.

Through the optimization of film diffusion and CO_2 dissolution, the addition of external recycles and the external dissolution of CO_2 improved the mass transfer of reactants and increased the availability of dissolved CO_2 at the catalyst surface, leading to improved reaction kinetics resulting redox current. Optimizing the electrocatalyst configuration by changing from TiO_2 and copper electrodes to platinum and copper wires improved the stability of current readings. In total, these changes increased the average current density during CO_2 saturation from -1,4 $\mu A/cm^2$ to -2,6*10^2 $\mu A/cm^2$.

Investigating the effects of external potential on current density and H_2/CO selectivity revealed that tuning the external potential offers significant control over the reaction kinetics and product distribution. By varying the potential, it becomes possible to influence the activation barriers and favour specific reaction pathways, thereby impacting the selectivity and yield of CO and hydrocarbons. Optimal selectivity towards CO production was identified at -1 V (vs Ag/AgCl). However, the choice of external potential must be carefully considered to strike a balance between driving the desired reactions and minimizing unwanted side reactions. While higher overpotentials may enhance reaction rates, they can also lead to increased energy consumption and undesirable side reactions. In this regard, techniques like chronoamperometry experiments play a vital role in understanding the electrochemical behaviour and identifying the potential ranges where the desired products are formed most efficiently.

Furthermore, four different electrolytes (KI, KI+Na_2CO_3/$NaHCO_3$, Na_2CO_3/$NaHCO_3$, and Na_2SO_4) were evaluated, considering their effects on current density, product selectivity, and stability. Chronoamperometry experiments provided valuable insights into the electrochemical behaviour of electrolytes. The carbon reduction current, observed upon CO_2 saturation, indicated the efficiency of CO_2 conversion. The electrolytes containing KI showed higher average currents and carbon reduction currents due to their high ionic conductivity. Based on a comprehensive comparison of electrolyte characteristics, KI was selected as the optimal electrolyte for analytical purposes in direct CO_2 reduction, considering its average current, carbon reduction current, current stability, pH, and CO/H_2 selectivity.

The optimization of TiO_2 catalyst loading showed that the catalyst layer thickness significantly affects the current response. An optimal catalyst thickness of 150 nm yielded the highest carbon reduction current. It was also found that UV-irradiation had no impact on the current and further analysis is recommended to understand the underlying mechanisms in more detail. Additionally, pH measurements suggested the presence of a CO_2 reduction chain where CO was formed as an intermediate.

Furthermore, it is noteworthy that GC-MS and FTIR measurements did not detect any hydrocarbons in the catholyte, despite indications of a carbon reduction chain. This suggests the formation of other intermediate species or the presence of highly volatile or unstable hydrocarbons

that were not captured by the analytical techniques used. In future research, the implementation of liquid chromatography analysis is recommended to gain a deeper understanding of the product selectivity and to identify any elusive hydrocarbon species. Ideally, this analysis setup features a bonded-phase silica column in conjunction with a nonpolar mobile phase. By employing more comprehensive characterization techniques, a more complete picture of the reaction pathways and product distributions can be obtained, enabling further optimization of the electrochemical CO_2 reduction process. To further enhance the efficiency of the CO_2 reduction process, it is recommended to decrease the distance between the cathodic and anodic electrocatalysts respectively. This can be achieved by implementing a downscaled version of the H-cell. Alternatively, changing the H-cell reactor design in favour of a flow reactor design can also offer a significant decrease in both electrocatalyst spacing, as well as decreased reactor volume.

References

[1] Debasish Sarkar, 21 - Energy Harvesters Based on Zinc Oxide, Editor(s): Kamlendra Awasthi, In Metal Oxides, Nanostructured Zinc Oxide, Elsevier, Amsterdam, Netherlands, 2021, Pages 605-637, ISBN 9780128189009, https://doi.org/10.1016/B978-0-12-818900-9.00007-3.

[2] Ewelina Grabowska, Martyna Marchelek, Marta Paszkiewicz-Gawron, Adriana Zaleska-Medynska, 3 - Metal oxide photocatalysts, Editor(s): Adriana Zaleska-Medynska, In Metal Oxides, Metal Oxide-Based Photocatalysis, Elsevier, Amsterdam, Netherlands, 2018, Pages 51-209, ISBN 9780128116340, https://doi.org/10.1016/B978-0-12-811634-0.00003-2.

[3] Anna Gołąbiewska, Marek P. Kobylański, Adriana Zaleska-Medynska, 2 - Fundamentals of metal oxide-based photocatalysis, Editor(s): Adriana Zaleska-Medynska, In Metal Oxides, Metal Oxide-Based Photocatalysis, Elsevier, Amsterdam, Netherlands, 2018, Pages 3-50, ISBN 9780128116340, https://doi.org/10.1016/B978-0-12-811634-0.00002-0.

[4] Prabhakarn Arunachalam, Abdullah M. Al Mayouf, Chapter 28 - Photoelectrochemical Water Splitting,Editor(s): Satyabrata Mohapatra, Tuan Anh Nguyen, Phuong Nguyen-Tri, In Micro and Nano Technologies, Noble Metal-Metal Oxide Hybrid Nanoparticles, Woodhead Publishing, Duxford, United Kingdom, 2019, Pages 585-606, ISBN 9780128141342, https://doi.org/10.1016/B978-0-12-814134-2.00028-0.

[5] N.R. Khalid, Ejaz Ahmed, M.B. Tahir, T. Iqbal, Sadia Khalid, Waqar Ahmed, Chapter 12 - Metal oxide semiconductors for photoelectrochemical water splitting, Editor(s): Waqar Ahmed, Matthew Booth, Ehsan Nourafkan, In Micro and Nano Technologies, Emerging Nanotechnologies for Renewable Energy, Elsevier, 2021, Pages 287-309, ISBN 9780128213469, https://doi.org/10.1016/B978-0-12-821346-9.00004-3.

[6] Hongwen Zhang, Jinlin Long, Chapter 9 - Photoelectrochemical reduction of carbon dioxide, Editor(s): Phuong Nguyen Tri, Haobin Wu, Tuan Anh Nguyen, Simon Barnabé, Pierre Bénard, In Micro and Nano Technologies, Nanomaterials for CO2 Capture, Storage, Conversion and Utilization, Elsevier, 2021, Pages 197-210, ISBN 9780128228944, https://doi.org/10.1016/B978-0-12-822894-4.00008-3.

[7] P.J. Kulesza, I.A. Rutkowska, A. Wadas,Electrocatalytic and Photoelectrochemical Reduction of Carbon Dioxide in Aqueous Media: Toward Generation of Fuels and Utility Chemicals, Editor(s): Klaus Wandelt, Encyclopedia of Interfacial Chemistry, Elsevier, Amsterdam, Netherlands, 2018, Pages 521-530, ISBN 9780128098943, https://doi.org/10.1016/B978-0-12-409547-2.14132-0.

[8] Yufei Jia, Fei Li, Ke Fan, Licheng Sun, Cu-based bimetallic electrocatalysts for CO2 reduction, Advanced Powder Materials, Volume 1, Issue 1, 2022, 100012, ISSN 2772-834X, https://doi.org/10.1016/j.apmate.2021.10.003.

[9] Pupo, Marilia & Kortlever, Ruud. (2019). Electrolyte Effects on the Electrochemical Reduction of CO2. ChemPhysChem. 20. 1-11. 10.1002/cphc.201900680.

[10] Xi Wu, Feiyu Kang, Wenhui Duan, Jia Li, Density functional theory calculations: A powerful tool to simulate and design high-performance energy storage and conversion materials, Progress in Natural Science: Materials International, Volume 29, Issue 3, 2019, Pages 247-255, ISSN 1002-0071, https://doi.org/10.1016/j.pnsc.2019.04.003.

[11] Qing Huang, Qiang Li, Jiang Liu, Yi–Rong Wang, Rui Wang, Long–Zhang Dong, Yu–Han Xia, Jin–Lan Wang, Ya-Qian Lan, Disclosing CO2 Activation Mechanism by Hydroxyl-Induced Crystalline Structure Transformation in Electrocatalytic Process, Matter, Volume 1, Issue 6, 2019, Pages 1656-1668, ISSN 2590-2385, https://doi.org/10.1016/j.matt.2019.07.003.

[12] Ziemba, Marc & Hess, Christian. (2023). Unravelling the mechanism of CO 2 activation over low-loaded Cu/CeO 2 (111) catalysts using operando and transient spectroscopies. Catalysis Science & Technology. 13. 10.1039/D3CY00494E.

[13] Qing Huang, Qiang Li, Jiang Liu, Yi–Rong Wang, Rui Wang, Long–Zhang Dong, Yu–Han Xia, Jin–Lan Wang, Ya-Qian Lan, Disclosing CO2 Activation Mechanism by Hydroxyl-Induced Crystalline Structure Transformation in Electrocatalytic Process, Matter, Volume 1, Issue 6, 2019, Pages 1656-1668, ISSN 2590-2385, https://doi.org/10.1016/j.matt.2019.07.003.

[14] Longmei Shang, Ximeng Lv, Hao Shen, Zhengzhong Shao, Gengfeng Zheng, Selective carbon dioxide electroreduction to ethylene and ethanol by core-shell copper/cuprous oxide, Journal of Colloid and Interface Science, Volume 552, 2019, Pages 426-431, ISSN 0021-9797, https://doi.org/10.1016/j.jcis.2019.05.073.

[15] Gao, Dunfeng & McCrum, Ian & Deo, Shyam & Choi, Yong-Wook & Scholten, Fabian & Wan, Weiming & Chen, Jingguang & Janik, Michael & Roldan Cuenya, Beatriz. (2018). Activity and Selectivity Control in CO2 Electroreduction to Multicarbon Products over CuOx Catalysts via Electrolyte Design. ACS Catalysis. 8. 10012-10020. 10.1021/acscatal.8b02587.

[16] Kortlever, Ruud & Shen, Jing & Schouten, K J P & Calle-Vallejo, Federico & Koper, Marc. (2015). Catalysts and Reaction Pathways for the Electrochemical Reduction of Carbon Dioxide. The Journal of Physical Chemistry Letters. 6. 150924081507003. 10.1021/acs.jpclett.5b01559.

[17] Zhenyu Sun, Tao Ma, Hengcong Tao, Qun Fan, Buxing Han, Fundamentals and Challenges of Electrochemical CO2 Reduction Using Two-Dimensional Materials, Chem, Volume 3, Issue 4, 2017, Pages 560-587, ISSN 2451-9294, https://doi.org/10.1016/j.chempr.2017.09.009.

[18] Lu, Q., Rosen, J., Zhou, Y. et al. A selective and efficient electrocatalyst for carbon dioxide reduction. Nat Commun 5, 3242 (2014). https://doi.org/10.1038/ncomms4242

[19] Baruch, Maor & Pander, James & White, James & Bocarsly, Andrew. (2015). Mechanistic Insights into the Reduction of CO2 on Tin Electrodes using In situ ATR-IR Spectroscopy. ACS Catalysis. 5. 150413134326004. 10.1021/acscatal.5b00402.

[20] White, James & Baruch, Maor & Pander, James & Hu, Yuan & Fortmeyer, Ivy & Park, James & Zhang, Tao & Liao, Kuo & Gu, Jing & Yan, Yong & Shaw, Travis & Abelev, Esta & Bocarsly, Andrew. (2015). Light-Driven Heterogeneous Reduction of Carbon Dioxide: Photocatalysts and Photoelectrodes. Chemical reviews. 115. 10.1021/acs.chemrev.5b00370.

[21] Peterson, Andrew & Abild-Pedersen, Frank & Studt, Felix & Rossmeisl, Jan & Nørskov, Jens. (2010). How copper catalyzes the electroreduction of carbon dioxide into hydrocarbon fuels. Energy & Environmental Science - ENERGY ENVIRON SCI. 3. 10.1039/c0ee00071j.

[22] Nie, Xiaowa & Esopi, Monica & Janik, Michael & Asthagiri, Aravind. (2013). Selectivity of CO2 Reduction on Copper Electrodes: The Role of the Kinetics of Elementary Steps. Angewandte Chemie (International ed. in English). 125. 10.1002/anie.201208320.

[23] DeWulf, D.W., Jin, T. and Bard, A.J., 1989. Electrochemical and surface studies of carbon dioxide reduction to methane and ethylene at copper electrodes in aqueous solutions. *Journal of the Electrochemical Society*, *136*(6), p.1686.

[24] Kuhl, Kendra & Hatsukade, Toru & Cave, Etosha & Abram, David & Kibsgaard, Jakob & Jaramillo, Thomas. (2014). Electrocatalytic Conversion of Carbon Dioxide to Methane and Methanol on Transition Metal Surfaces. Journal of the American Chemical Society. 136. 10.1021/ja505791r.

[25] Cruz, Pamela & Irikura, Kallyni & Lachgar, Abdessadek & Cardoso, Juliano & Alarcón, Hugo & Zanoni, Maria. (2020). Preparation of FTO/CU2O Electrode Protected by PEDOT:PSS and Its Better Performance in the Photoelectrocatalytic Reduction of CO2 to Methanol. Electrocatalysis. 11. 10.1007/s12678-020-00612-z.

[26] Hori, Yoshio & Takahashi, Ichiro & Koga, Osamu & Hoshi, Nagahiro. (2002). Selective Formation of C2 Compounds from Electrochemical Reduction of CO 2 at a Series of Copper Single Crystal Electrodes. Journal of Physical Chemistry B - J PHYS CHEM B. 106. 15-17. 10.1021/jp013478d.

[27] Yang, Ki & Lee, Chan & Jin, Kyoungsuk & Im, Sang & Nam, Ki Tae. (2017). Current Status and Bioinspired Perspective of Electrochemical Conversion of CO 2 to Long Chain Hydrocarbon. The Journal of Physical Chemistry Letters. 8. 10.1021/acs.jpclett.6b02748.

[28] Christoph J. Bondue, Matthias Graf, Akansha Goyal, and Marc T. M. Koper*, Journal of the American Chemical Society* 2021 *143* (1), 279-285, DOI: 10.1021/jacs.0c10397

[29] Ulejczyk, Bogdan & Jóźwik, Paweł & Młotek, Michał & Krawczyk, Krzysztof. (2022). A Promising Cobalt Catalyst for Hydrogen Production. Catalysts. 12. 10.3390/catal12030278.

[30] Kang, Xinchen & Zhu, Qinggong & Sun, Xiaofu & Hu, Jiayin & Zhang, Jianling & Liu, Zhimin & Han, Buxing. (2015). Highly Efficient Electrochemical Reduction of CO2 to CH4 in Ionic Liquid using Metal-Organic Framework Cathode. Chem. Sci. 7. 10.1039/C5SC03291A.

[31] Kibria, Md & Edwards, Jonathan & Gabardo, Christine & Dinh, Cao Thang & Seifitokaldani, Ali & Sinton, David & Sargent, Edward. (2019). Electrochemical CO 2 Reduction into Chemical Feedstocks: From Mechanistic Electrocatalysis Models to System Design. Advanced Materials. 31. 1807166. 10.1002/adma.201807166.

[32] Wakerley, David & Lamaison, Sarah & Wicks, Joshua & Clemens, Auston & Feaster, Jeremy & Corral, Daniel & Jaffer, Shaffiq & Sarkar, Amitava & Fontecave, Marc & Duoss, Eric & Baker, Sarah & Sargent, Edward & Jaramillo, Thomas & Hahn, Christopher. (2022). Gas diffusion electrodes, reactor designs and key metrics of low-temperature CO2 electrolysers. Nature Energy. 7. 1-14. 10.1038/s41560-021-00973-9.

[33] Sassenburg, Mark & Rooij, Reinier & Nesbitt, Nathan & Kas, Recep & Chandrashekar, Sanjana & Firet, Nienke & Yang, Kailun & Liu, Kai & Blommaert, Marijn & Kolen, Martin & Ripepi, Davide & Smith, Wilson & Burdyny, Tom. (2022). Characterizing CO 2 Reduction Catalysts on Gas Diffusion Electrodes: Comparing Activity, Selectivity, and Stability of Transition Metal Catalysts. ACS Applied Energy Materials. 5. 10.1021/acsaem.2c00160.

[34] Hernandez Aldave, Sandra & Andreoli, Enrico. (2020). Fundamentals of Gas Diffusion Electrodes and Electrolysers for Carbon Dioxide Utilisation: Challenges and Opportunities. Catalysts. 10. 713. 10.3390/catal10060713.

[35] Yu Yang, Fengwang Li, Reactor design for electrochemical CO2 conversion toward large-scale applications, Current Opinion in Green and Sustainable Chemistry, Volume 27, 2021, 100419, ISSN 2452-2236, https://doi.org/10.1016/j.cogsc.2020.100419.

[36] Gu, Yueyuan & Wei, Jucai & Li, Jindong & Wang, Luyang & Wu, Xu. (2021). Long-Term-Stable Continuous Flow CO2 Reduction Electrolysers with High Current Efficiency. Sustainable Energy & Fuels. 5. 10.1039/D0SE01707H.

[37] Danish, Mir Sayed Shah & Estrella - Pajulas, Liezel & Alemaida, Ivy & Lisin, Anton & Moiseev, Nikita & Ahmadi, Mikaeel & Nazari, Massoma & Wali, Mohebullah & Zaheb, Hameedullah & Senjyu, Tomonobu. (2021). Photocatalytic Applications of Metal Oxides for Sustainable Environmental Remediation. Metals - Open Access Metallurgy Journal. 11. 80. 10.3390/met11010080.

[38] Parashar, Mritunjaya & Shukla, Vivek & Singh, Ranbir. (2020). Metal oxides nanoparticles via sol–gel method: a review on synthesis, characterization and applications. Journal of Materials Science: Materials in Electronics. 31. 10.1007/s10854-020-02994-8.

[39] Tao, Zixu & Wu, Zishan & Yuan, Xiaolei & Wu, Yueshen & Wang, Hailiang. (2019). Copper-Gold Interactions Enhancing Formate Production from Electrochemical CO2 Reduction. ACS Catalysis. 2019. 10.1021/acscatal.9b03158.

[40] Dina Ewis, Muhammad Arsalan, Mazen Khaled, Deepak Pant, Muneer M. Ba-Abbad, Abdulkarem Amhamed, Muftah H. El-Naas, Electrochemical reduction of CO2 into

formate/formic acid: A review of cell design and operation, Separation and Purification Technology, Volume 316, 2023, 123811, ISSN 1383-5866, https://doi.org/10.1016/j.seppur.2023.123811.

[41] Xin Li, Song Hong, Leiduan Hao, Zhenyu Sun, Cadmium-based metal–organic frameworks for high-performance electrochemical CO2 reduction to CO over wide potential range, Chinese Journal of Chemical Engineering, Volume 43, 2022, Pages 143-151, ISSN 1004-9541, https://doi.org/10.1016/j.cjche.2021.10.013.

[42] Shaughnessy, Charles & Jantz, Dylan & Leonard, Kevin. (2017). Selective Electrochemical CO2 Reduction to CO Using In-Situ Reduced In2O3 Nanocatalysts. J. Mater. Chem. A. 5. 10.1039/C7TA06570A.

[43] Juliana Alves Silva, João Batista Oliveira Santos, Daniel Torres, José Luis Pinilla, Isabel Suelves, Natural Fe-based catalysts for the production of hydrogen and carbon nanomaterials via methane decomposition, International Journal of Hydrogen Energy, Volume 46, Issue 71, 2021, Pages 35137-35148, ISSN 0360-3199, https://doi.org/10.1016/j.ijhydene.2021.08.065.

[44] D.H. Bradhurst, P.M. Heuer, G.Z.A. Stolarski, Hydrogen production and storage using titanium electrodes and metal hydrides, International Journal of Hydrogen Energy, Volume 8, Issue 2, 1983, Pages 85-90, ISSN 0360-3199, https://doi.org/10.1016/0360-3199(83)90090-3.

[45] Kitano, M. & Tsujimaru, K. & Anpo, M.. (2008). Hydrogen Production Using Highly Active Titanium Oxide-based Photocatalysts. Topics in Catalysis. 49. 4-17. 10.1007/s11244-008-9059-2.

[46] Lee, Dong & Dongjoon, Min. (2019). A Kinetics of Hydrogen Reduction of Nickel Oxide at Moderate Temperature. Metals and Materials International. 25. 10.1007/s12540-019-00261-y.

[47] Manukyan, Khachatur & Avetisyan, Arpi & Shuck, Christopher & Chatilyan, Hakob & Rouvimov, Sergei & Kharatyan, Suren & Kharatyan, L & Mukasyan, A.. (2015). Nickel Oxide Reduction by Hydrogen: Kinetics and Structural Transformations. The Journal of Physical Chemistry C. 119. 16131–16138. 10.1021/acs.jpcc.5b04313.

[48] Wan, Lili & Zhang, Xilin & Cheng, Jinshui & Chen, Rong & Wu, Linxiao & Shi, Jiawen & Luo, Jingshan. (2022). Bimetallic Cu–Zn Catalysts for Electrochemical CO 2 Reduction: Phase-Separated versus Core–Shell Distribution. ACS Catalysis. 12. 2741-2748. 10.1021/acscatal.1c05272.

[49] Chen, Wei & Wang, Yating & Li, Yuhang & Li, Chunzhong. (2022). Electrocatalytic CO 2 Reduction over Bimetallic Bi-Based Catalysts: A Review. CCS Chemistry. 5. 1-24. 10.31635/ccschem.022.202202357.

[50] Ma, Sichao & Sadakiyo, Masaaki & Heima, Minako & Luo, Raymond & Haasch, Richard & Gold, Jake & Yamauchi, Miho & Kenis, Paul. (2016). Electroreduction of Carbon Dioxide to Hydrocarbons Using Bimetallic Cu-Pd Catalysts with Different Mixing Patterns. Journal of the American Chemical Society. 139. 10.1021/jacs.6b10740.

[51] Mistry, Hemma & Reske, Rulle & Strasser, Peter & Roldan Cuenya, Beatriz. (2016). Size-dependent reactivity of gold-copper bimetallic nanoparticles during CO2 electroreduction. Catalysis Today. 288. 10.1016/j.cattod.2016.09.017.

[52] Wang, Yuanxing & Niu, Cailing & Zhu, Yachuan. (2019). Copper–Silver Bimetallic Nanowire Arrays for Electrochemical Reduction of Carbon Dioxide. Nanomaterials. 9. 173. 10.3390/nano9020173.

[53] Narváez-Celada, Denise & Varela Gasque, Ana Sofia. (2022). CO 2 electrochemical reduction on metal–organic framework catalysts: current status and future directions. Journal of Materials Chemistry A. 10. 10.1039/D1TA10440C.

[54] Kornienko, Nikolay & Zhao, Yingbo & Kley, Christopher & Zhu, Chenhui & Kim, Dohyung & Lin, Song & Chang, Christopher & Yaghi, Omar & Yang, Peidong. (2015). Metal-Organic Frameworks for Electrocatalytic Reduction of Carbon Dioxide. Journal of the American Chemical Society. 137. 10.1021/jacs.5b08212.

[55] Wang, Xuanyu & Zou, Yanhong & Zhang, Yan Xing & Marchetti, Barbara & Liu, Yuyu & Yi, Jin & Zhou, Xiao-Dong & Zhang, Jiujun. (2022). Tin-based Metal Organic Framework Catalysts for High-Efficiency Electrocatalytic CO2 Conversion into Formate. Journal of Colloid and Interface Science. 626. 10.1016/j.jcis.2022.07.008.

[56] Li Tan, Yanru Li, Qian Lv, Yuyan Gan, Yuan Fang, Yu Tang, Lizhi Wu, Yuanxing Fang, Development of soluble UiO-66 to improve photocatalytic CO2 reduction, Catalysis Today, Volume 410, 2023, Pages 282-288, ISSN 0920-5861, https://doi.org/10.1016/j.cattod.2022.05.001.

[57] Shreya Mahajan, Manu Lahtinen, Recent progress in metal-organic frameworks (MOFs) for CO2 capture at different pressures, Journal of Environmental Chemical Engineering, Volume 10, Issue 6, 2022, 108930, ISSN 2213-3437, https://doi.org/10.1016/j.jece.2022.108930.

[58] Xi-Qing Wang, Qin Chen, Ya-Jiao Zhou, Hong-Mei Li, Jun-Wei Fu, Min Liu, Cu-based bimetallic catalysts for CO2 reduction reaction, Advanced Sensor and Energy Materials, Volume 1, Issue 3, 2022, 100023, ISSN 2773-045X, https://doi.org/10.1016/j.asems.2022.100023.

[59] Dong Jiang, Ran Bu, Wei Xia, Yichen Hu, Mengchen Zhou, Enqing Gao, Toru Asahi, Yusuke Yamauchi, Jing Tang, Cobalt phthalocyanine-based conjugated polymer as efficient and exclusive electrocatalyst for CO2 reduction to ethanol, Materials Reports: Energy, Volume 3, Issue 1, 2023, 100176, ISSN 2666-9358, https://doi.org/10.1016/j.matre.2023.100176.

[60] Pan, Fuping & Yang, Yang. (2020). Designing CO2 Reduction Electrode Materials by Morphology and Interface Engineering. Energy & Environmental Science. 13. 10.1039/D0EE00900H.

[61] Huygh, Stijn & Bogaerts, Annemie & Neyts, Erik. (2016). How Oxygen Vacancies Activate CO 2 Dissociation on TiO 2 Anatase (001). The Journal of Physical Chemistry C. 120. 10.1021/acs.jpcc.6b07459.

[62] Takahashi, H. & Liu, Lihui & Yashiro, Y. & Ioku, Koji & Bignall, Greg & Yamasaki, N. & Kori, T. (2006). CO2 reduction using hydrothermal method for the selective formation of organic compounds. Journal of Materials Science. 41. 1585-1589. 10.1007/s10853-006-4649-5.

[63] Yan Huo, Shijian Xiu, Long-Yue Meng, Bo Quan, Solvothermal synthesis and applications of micro/nano carbons: A review, Chemical Engineering Journal, Volume 451, Part 2, 2023, 138572, ISSN 1385-8947, https://doi.org/10.1016/j.cej.2022.138572.

[64] Dias, Eduardo & Silva, Gelson & Cruz, Jean & Ribeiro, Caue. (2022). One-Pot Solvothermal Synthesis of Carbon Black-Supported CuO for Catalysis of CO 2 Electroreduction. ChemElectroChem. 9. 10.1002/celc.202200206.

[65] Ye Xiaodong, Jiang Yangyang, Chen Xi, Guo Benshuai, Mao Songbai, Guo Yafei, Zhao Chuanwen, Insights Into the Template Effect on Nanostructured CuO Catalysts for Electrochemical CO2 Reduction to CO, Frontiers in Energy Research, Volume 10, 2022, 10.3389/fenrg.2022.964011, https://www.frontiersin.org/articles/10.3389/fenrg.2022.964011, 2296-598X.

[66] Rahman, Rasha & Menamparambath, Mini. (2020). Soft-template-assisted synthesis: A promising approach for the fabrication of transition metal oxides. Nanoscale Advances. 2. 5015. 10.1039/d0na00599a.

[67] Varela Gasque, Ana Sofia & Ju, Wen & Bagger, Alexander & Franco, Patricio & Rossmeisl, Jan & Strasser, Peter. (2019). Electrochemical reduction of CO2 (CO2RR) on Metal-Nitrogen-doped carbon (MNC) catalysts. ACS Catalysis. 9. 10.1021/acscatal.9b01405.

[68] Fangqi Yang, Haoming Yu, Xinyu Mao, Qiangguo Meng, Shixia Chen, Qiang Deng, Zheling Zeng, Jun Wang, Shuguang Deng, Boosting electrochemical CO2 reduction on ternary heteroatoms-doped porous carbon, Chemical Engineering Journal, Volume 425, 2021, 131661, ISSN 1385-8947, https://doi.org/10.1016/j.cej.2021.131661.

[69] Lontio Fomekong, Roussin & Saruhan, Bilge. (2019). Synthesis of Co 3+ Doped TiO 2 by Co-precipitation Route and Its Gas Sensing Properties. Frontiers in Materials. 6. 252. 10.3389/fmats.2019.00252.

[70] Abbas, M. & RASHEED, Mohammed. (2021). Solid State Reaction Synthesis and Characterization of Cu doped TiO 2 Nanomaterials. Journal of Physics: Conference Series. 1795. 012059. 10.1088/1742-6596/1795/1/012059.

[71] Yiqiang Jiang, Changhyeok Choi, Song Hong, Senlin Chu, Tai-Sing Wu, Yun-Liang Soo, Leiduan Hao, Yousung Jung, Zhenyu Sun, Enhanced electrochemical CO2 reduction to ethylene over CuO by synergistically tuning oxygen vacancies and metal doping,Cell Reports Physical Science, Volume 2, Issue 3, 2021, 100356, ISSN 2666-3864, https://doi.org/10.1016/j.xcrp.2021.100356.

[72] Linghao Zhu, Cong Qin, Yan Wang, Jianliang Cao, Single-atom Pt supported on non-metal doped WS2 for photocatalytic CO2 reduction: A first-principles study, Applied Surface Science, Volume 626, 2023, 157252, ISSN 0169-4332, https://doi.org/10.1016/j.apsusc.2023.157252.

[73] Sikam, Pornsawan & Jitwatanasirikul, Thanadol & Roongcharoen, Thantip & Yodsin, Nuttapon & Meeprasert, Jittima & Takahashi, Kaito & Namuangruk, Supawadee. (2022). Understanding the interaction between transition metal doping and ligand atoms of ZnS and ZnO monolayers to promote CO 2 reduction reaction. Physical Chemistry Chemical Physics. 24. 10.1039/D2CP00878E.

[74] Zhang, Jingzhao & Tse, Kinfai & Wong, Manhoi & Zhang, Yiou & Zhu, Junyi. (2016). A brief review of co-doping. Frontiers of Physics. 11. 1-21. 10.1007/s11467-016-0577-2.

[75] Kas, Recep & Yang, Kailun & Bohra, Divya & Kortlever, Ruud & Burdyny, Tom & Smith, Wilson. (2019). Electrochemical CO2 Reduction on Nanostructured Metal Electrodes: Fact or Defect?. 10.26434/chemrxiv.10032278.

[76] Köhler, Johann & Fritzsche, Wolfgang. (2007). Nanotechnology: An Introduction to Nanostructuring Techniques. 10.1002/9783527621132.

[77] Janik, Michael & Neurock, Matthew. (2007). A first principles analysis of the electro-oxidation of CO over Pt(111). Electrochimica Acta. 52. 5517-5528. 10.1016/j.electacta.2007.01.060.

Appendices

Appendix A: Overview of chrono amperometry measurements conducted at varying voltages.

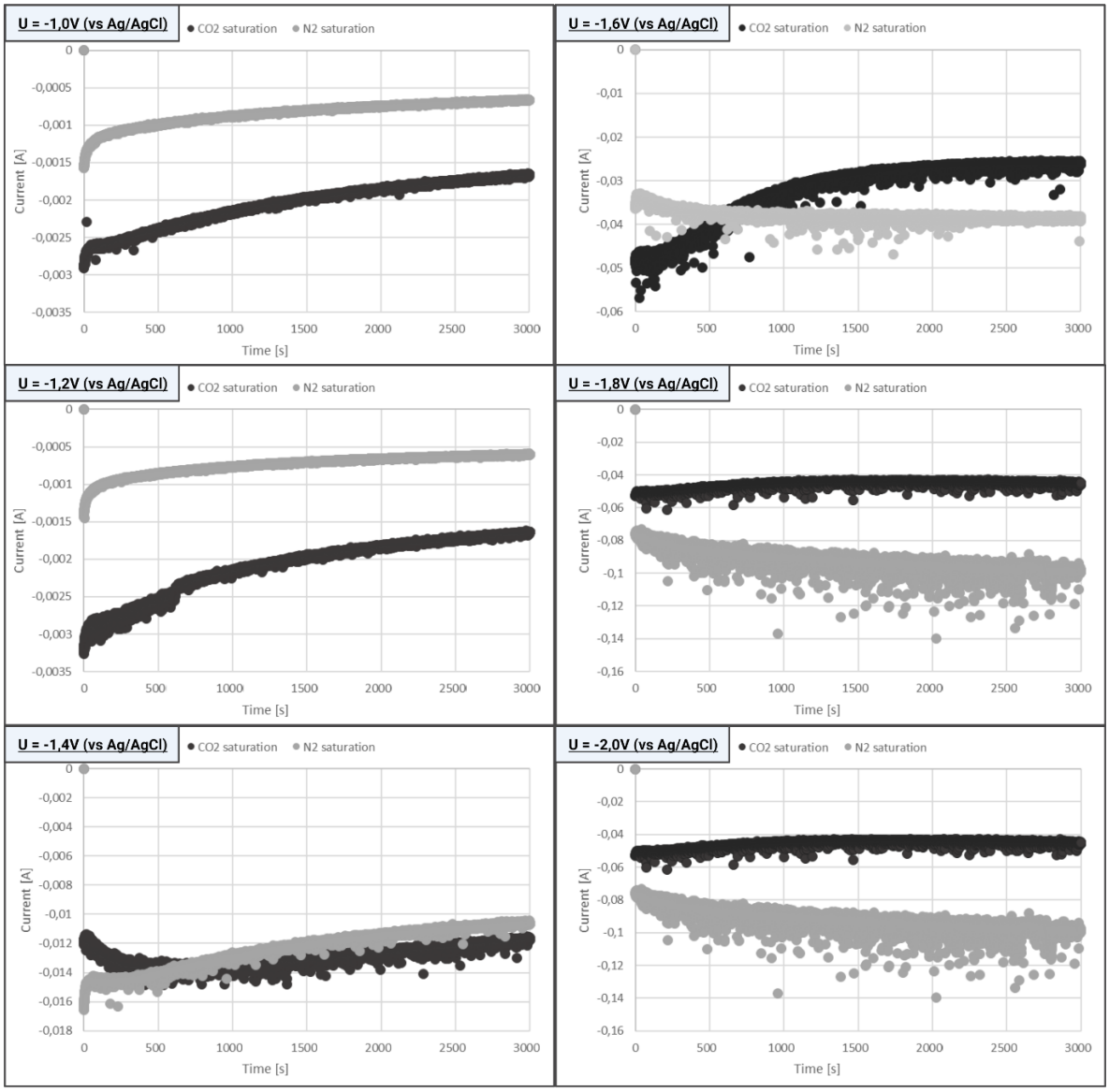

Appendix B: Overview of chrono amperometry measurements conducted with varying electrolyte composition.

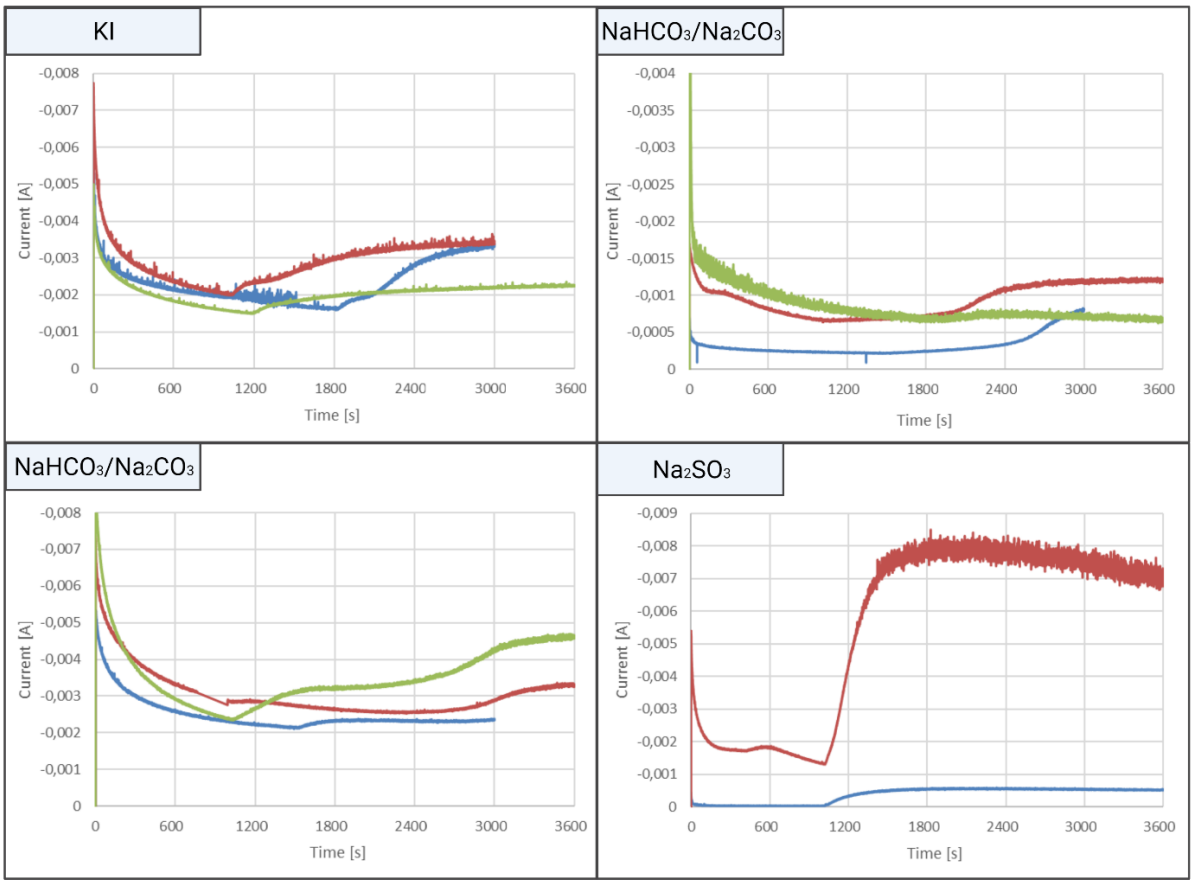

Appendix C: Overview of chrono amperometry measurements conducted with varying TiO_2 layer thickness.